Journal Pre-proofs

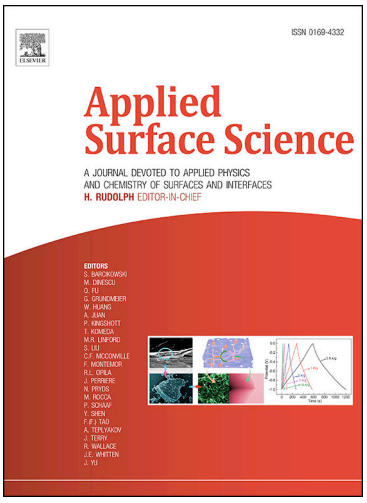

Full Length Article

Low-temperature atmospheric pressure plasma deposition of TiO_2-based nanocomposite coatings on open-cell polymer foams for photocatalytic water treatment

Antonella Uricchio, Elie Nadal, Beatrice Plujat, Gael Plantard, Françoise Massines, Fiorenza Fanelli

PII: S0169-4332(21)01090-4
DOI: https://doi.org/10.1016/j.apsusc.2021.150014
Reference: APSUSC 150014

To appear in: *Applied Surface Science*

Received Date: 21 January 2021
Revised Date: 16 April 2021
Accepted Date: 30 April 2021

Please cite this article as: A. Uricchio, E. Nadal, B. Plujat, G. Plantard, F. Massines, F. Fanelli, Low-temperature atmospheric pressure plasma deposition of TiO_2-based nanocomposite coatings on open-cell polymer foams for photocatalytic water treatment, *Applied Surface Science* (2021), doi: https://doi.org/10.1016/j.apsusc.2021.150014

Low-temperature atmospheric pressure plasma deposition of TiO_2-based nanocomposite coatings on open-cell polymer foams for photocatalytic water treatment

Antonella Uricchio[a], Elie Nadal[b,c], Beatrice Plujat[b,c], Gael Plantard[b,c,*], Françoise Massines[c], Fiorenza Fanelli[d,*]

Antonella Uricchio:, Investigation, Data curation, Visualization, Writing-Original draft preparation

Elie Nadal: Investigation, Data curation

Beatrice Plujat: Investigation

Gael Plantard: Conceptualization, Methodology, Validation, Writing-Reviewing and Editing

Françoise Massines: Methodology, Validation, Supervision

Fiorenza Fanelli: Conceptualization, Methodology, Validation, Supervision, Writing-Reviewing and Editing

Graphical abstract

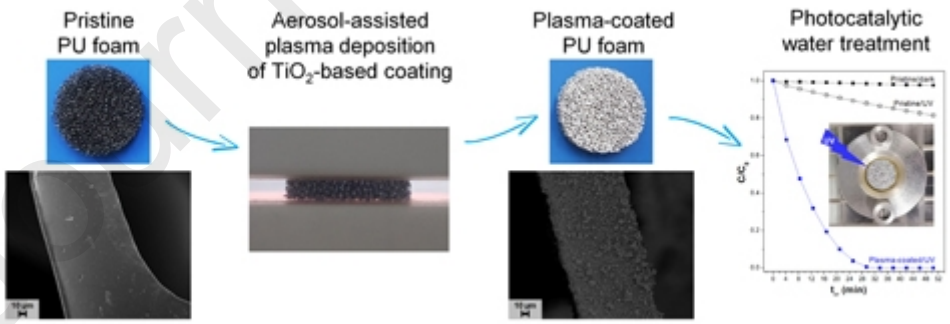

(color online only)

Highlights

- Photocatalytic TiO_2-based films are deposited by atmospheric pressure cold plasma
- Films are deposited on open-cell polyurethane foams and flat glass slides

- The plasma process allows the controlled deposition on complex 3D porous materials
- The plasma-coated materials present good photocatalytic activity and reusability
- The evolution of the photocatalytic materials upon use in photocatalysis is studied

[a]Department of Chemistry, University of Bari 'Aldo Moro', via Orabona 4, 70126 Bari, Italy

[b]Laboratoire Procédés Matériaux et Energie Solaire, PROMES-CNRS, UPR 8521, Technosud, Rambla de la thermodynamique, 66100 Perpignan, France

[c]University of Perpignan Via Domitia, 52 avenue Paul Alduy, 66100 Perpignan, France

[d]National Research Council (CNR), Institute of Nanotechnology (NANOTEC), c/o Department of Chemistry, University of Bari 'Aldo Moro', via Orabona 4, 70126 Bari, Italy

*Corresponding authors at :

- Institute of Nanotechnology (NANOTEC), National Research Council, c/o Department of Chemistry, University of Bari "Aldo Moro", via Orabona 4, 70126 Bari, Italy.

  E-mail address: fiorenza.fanelli@cnr.it (F. Fanelli).

  Phone: +39 0805442227
- PROcédés, Matériaux et Energies Solaires, UPR-8521 (CNRS), Tecnosud, Rambla de la thermodynamique, 66100 Perpignan

  E-mail address: plantard@univ-perp.fr (G. Plantard).

  Phone: +33 0612524782

ABSTRACT

An aerosol-assisted plasma process was used to deposit, at low temperature and atmospheric pressure, photocatalytic hydrocarbon polymer/TiO_2 nanoparticles nanocomposite coatings onto

both flat glass slides and open-cell polyurethane foams. Various characterization techniques were used to demonstrate the potential of the developed process for the controlled deposition of TiO_2-based coatings on the different supporting substrates, with special attention to the foams due to their complex three-dimensional porous structure.

The photocatalytic activity of the plasma-coated materials was evaluated by the decomposition of methyl orange in aqueous solution under UV irradiation, using a purposely designed recirculating batch photoreactor. The comparative study revealed that greater photocatalytic activity can be achieved with the open-cell foams, pointing to the beneficial properties of macroporous photocatalyst supports in comparison with conventional flat ones.

The prepared photocatalytic materials presented remarkable reusability and maintained good activity after prolonged operation (40 h) corresponding to 20 consecutive reaction runs. Results on the evolution of the photocatalytic performance of the plasma-coated samples over multiple runs were correlated with those obtained from the detailed characterization of their surface chemical composition, morphology and wettability as a function of the operation time in photocatalytic water treatment.

KEYWORDS

Photocatalytic coating

Titanium dioxide nanoparticles

Atmospheric pressure plasma deposition

Open-cell polymer foam

Water remediation

Dielectric barrier discharge

1. INTRODUCTION

The design and preparation of photocatalytic materials for the degradation of organic pollutants in water has attracted considerable interest during the last decades [1,2]. Research in this field has long been dominated by the use of freely suspended nano- and microparticles of

semiconductor metal oxides, due to the high surface-to-volume ratios and mass transfer rates offered by well-mixed slurry photocatalytic systems [1–5]. However, over the years, ever-increasing efforts have been devoted to achieve the permanent and efficient immobilization of photocatalysts onto suitable supports [2,4–8]. Interestingly, photocatalyst immobilization not only facilitates the separation and recovery of the catalyst from the treated solution, but can also enable the operation of continuous-flow photocatalytic reactors [2,4–8]. Therefore, numerous studies have been focused, for instance, on the deposition of TiO_2-based thin films [6–7,9–20] (e.g., TiO_2 thin films and TiO_2-containing nanocomposite coatings) on many different immobilization supports, which include both inorganic and polymeric materials (e.g., glass, silica, carbon black, ceramics, natural and synthetic polymers) in various forms, such as plates, beads, granules, fibers, fabrics, membranes, foams, scaffolds, etc. [5,6,16,17,20–22]. Among others, three-dimensional (3D) macroporous supports (average pore size ranging from 50 nm to a few millimeters) have gained attention because they enable the development of photocatalytic materials with high active surface area per unit of photoreactor volume and low flow resistance [22–31]. For instance, it has been found that, due to their highly interconnected porous structure, photocatalyst-coated open-cell foams (e.g., ceramic, metal, or polymer foams coated with photocatalytic thin films) exhibit large interface for reaction and superior light-harnessing capabilities, while allowing polluted water to flow through efficiently [22–37]. As a consequence, they are able to significantly exceed the overall photocatalytic performances obtained by using conventional flat supports (often referred to as two-dimensional supports) [27,28]. Indeed, with proper selection of the photoreactor architecture and operating conditions, photocatalyst-coated open-cell foams can even approximate the degradation efficiency of suspended photocatalyst nanopowders [23,27,28,32,38]. However, despite the above mentioned performances, it is widely acknowledged that the uniform and well-controlled deposition of photocatalytic thin films over the entire 3D structure of macroporous supports is a challenging task. Wet impregnation represents the most used strategy for such purpose. It

generally involves dipping the porous substrate into a nanocatalyst suspension, followed by drying at room or moderate temperature (commonly less than 150°C) and, in some cases, also by high-temperature calcination (400-900°C) [23–29,31–35]. Although impregnation is simple and inexpensive to implement, it does not allow a fine control of the growth of the photocatalytic layer. Moreover, when carried out in combination with heat treatments, it is not compatible with thermolabile supporting substrates (e.g., polymeric foams and scaffolds). The scientific literature also reports on the use of gas-phase techniques, such as atomic layer deposition (ALD) [30]. ALD offers tunable thin film composition, precise thickness control and exceptional conformality on both inorganic and polymeric substrates of complex geometry; however, it is characterized by low deposition rates [20,30]. Therefore, the development of novel strategies for the high-throughput controlled deposition of photocatalytic coatings on macroporous supports is highly desirable.

Recently, various atmospheric pressure (AP) low-temperature plasma processes have been optimized for the facile and efficient deposition of TiO_2-based thin films [9,14,39–44]. Proposed approaches include both classical plasma-enhanced chemical vapor deposition (PECVD) processes [9,14,41] and innovative aerosol-assisted plasma deposition (AAPD) strategies [40,42–44]. They exploit different direct [40,42,43] and remote [9,14,44] AP plasma sources operating close to room temperature and, therefore, suitable for the surface modification of both inorganic and polymeric materials. Various studies have demonstrated that the chemical composition and morphology of the deposited coatings can be easily adjusted by changing process parameters such as the plasma excitation conditions, the feed mixture composition and the deposition time [9,14,39–44]. However, a few papers have been published so far on the photocatalytic performances of the deposited coatings [9,41]. Moreover, to date, published studies have been mainly limited to the use of flat substrates and, therefore, additional efforts are still needed to achieve the deposition of well-structured TiO_2-based films on complex-geometry supports. Interestingly, in the last few years, AP low-temperature plasmas have been

successfully proposed for the surface modification of 3D porous materials [45–51]. It has been shown that, for instance, the careful optimization of the plasma reactor configuration and operating conditions can lead to the deposition of a thin film on both the outer and inner surfaces of the treated samples. Importantly, the overall uniformity of the plasma process over the entire sample can be remarkably improved by promoting plasma ignition or penetration throughout its porous structure [45–47].

In this work, an aerosol-assisted non-equilibrium plasma process was used to deposit, at low temperature and atmospheric pressure, TiO_2-containing thin films on both open-cell polyurethane (PU) foams and flat glass slides with the aim of developing novel photocatalytic materials. The choice of the PU foams was dictated by the fact that they are low-cost macroporous polymeric materials with good chemical and thermal resistance [5,35–37,52]. In addition, they present adequate mechanical strength and elasticity, which allow them to be easily shaped according to the photoreactor geometry [5,52].

In particular, in this work, hydrocarbon polymer/TiO_2 nanoparticles nanocomposite (NC) coatings were prepared by using a parallel-plate dielectric barrier discharge (DBD) fed with helium and the aerosol of dispersion of oleate-capped TiO_2 nanoparticles (NPs) in a hydrocarbon solvent mixture. During deposition, samples were placed in the middle of the discharge region, so that plasma ignition could be achieved also inside the porous structure of the foams [45]. The chemical composition and morphology of the plasma-coated materials were investigated by means of X-ray photoelectron spectroscopy (XPS), attenuated total reflectance-Fourier transform infrared spectroscopy (ATR-FTIR) and scanning electron microscopy (SEM), as a function of the process parameters, such as the deposition time and the NPs concentration in the starting dispersion. Among others, XPS and SEM analyses allowed assessing the overall uniformity of the deposition process on the 3D porous samples. The photocatalytic activity of plasma-coated glass slides and PU foams was compared by investigating the degradation of a model dye molecule (i.e., methyl orange, MO) in aqueous

solution, under UV irradiation. Photocatalytic experiments were carried out by using a recirculating flow reactor purposely designed for proper integration of the photocatalytic materials developed in this work. Finally, the recyclability of the best-performing samples was examined over 20 successive reaction runs. Findings were correlated with results from an in-depth investigation of the changes in the surface chemical composition, morphology and wettability as a function of the operation time in photocatalytic water treatment.

2. EXPERIMENTAL

2.1 Thin film deposition

Nanocomposite films were deposited by using a home-made atmospheric pressure dielectric barrier discharge (DBD) reactor, as previously described [53,54]. The apparatus consists of a parallel plate DBD cell, placed into an airtight Plexiglass chamber (Figs. 1 and S1). The plasma was generated between two dielectric-covered electrodes (50×50 mm^2 area, 4 mm gap) by applying a 22 kHz sinusoidal high voltage of 2.6 kV_{rms} in pulsed mode at modulation frequency and duty cycle of 50 Hz and 65%, respectively [53–54]. During the deposition processes, the plasma was fed with helium (Air Liquide, 99.999% purity) and the aerosol of a dispersion of oleate-capped TiO_2 NPs in a hydrocarbon solvent mixture of n-octane (Sigma-Aldrich, purity ≥ 99.0%,) and 1,7-octadiene (Sigma-Aldrich, 98% purity). The aerosol was generated using a TSI pneumatic atomizer (TSI, model 3076). The helium and dispersion flow rates were kept fixed at 8 slm and 0.22 ± 0.2 $g \cdot min^{-1}$, respectively. The above mentioned electrical and feed mixture conditions led to the ignition of a filamentary DBD with average specific power of 1.3 ± 0.1 $W \cdot cm^{-2}$. In particular, in this work, commercial Aeroxide® P25 TiO_2 NPs (Evonik Degussa GmbH, ≥99.5% purity) were utilized. They present an average particle size of about 30 nm and an anatase-to-rutile ratio of about 80:20 [55]. The NPs were first capped with oleate using a previously reported wet chemistry procedure [53], to obtain a stable dispersion in

hydrocarbon solvents. The concentration of NPs in the starting dispersion ([NPs]) was varied from 3 to 8 wt%, keeping constant the composition of the n-octane/1,7-octadiene mixture (i.e., 1,7-octadiene concentration of 0.5 vol%). The process duration (i.e., the deposition time, t_d) was varied in the range 10-60 min.

Thin films were deposited on (i) flat supports, i.e., round borosilicate glass slides (Agar) with diameter and thickness of 22 mm and 0.2 mm, respectively (Fig. 1b), and (ii) 3D macroporous supports, consisting of 4 mm thick round samples (22 mm diameter) of a commercial open-cell foam (Angst + Pfister) with polyester polyol-based polyurethane structure, pore density of 45 pores per inch (ppi) and porosity of ca. 97% (Fig. 1c). The flat and porous supports used in this work present significantly different surface area, which here is meant to indicate the surface area of the support available for coating deposition. Specifically, as discussed in the Supporting Information, the surface area of the foam samples (8400 mm^2) is about 22 times greater than that of the flat glass slides (380 mm^2) [28,56].

Deposition processes on the flat supports were carried out by placing two samples in the middle of the DBD region onto the dielectric plate covering the lower electrode. In case of the porous substrates, two foam samples were placed in the center of the discharge region and sandwiched between the two alumina plates covering the electrodes as shown in Fig. S1b. Using this arrangement, the feed mixture was forced to flow through the samples and plasma ignition was also obtained inside their porous structure (Fig. S1c).

2.2 Material characterization

X-ray photoelectron spectroscopy (XPS) analyses were performed by means of a PHI P5000 VersaProbe II scanning XPS microprobe spectrometer, while attenuate total reflectance-Fourier transform infrared (ATR-FTIR) spectra were collected using a vacuum Bruker Vertex 70v FTIR spectrometer. Details on measurements and data processing are provided in the Supporting Information.

X-ray diffraction (XRD) analyses of pristine TiO_2 NPs, oleate-capped TiO_2 NPs and NC coatings were performed on a PANalytical X'Pert MPD X-Ray diffractometer using a Cu Kα anode.

The weight of the coating deposited onto the various supporting substrates was measured by a Mettler Toledo XS205 analytical balance. The coating surface density, expressed in units of mass per unit area ($\mu g \cdot mm^{-2}$), was calculated by dividing the weight of the coating deposited onto the support by the support surface area. In addition, the mass deposition rate ($\mu g \cdot mm^{-2} \cdot min^{-1}$) was determined by dividing the coating surface density by the deposition time.

The morphology of the plasma-coated samples was investigated by a Zeiss SUPRA™ 40 field emission scanning electron microscope (FESEM) as described in the Supporting Information.

Samples wettability was evaluated by measuring the static water contact angle (WCA) with a KSV CAM 200 Instrument. Each WCA value is the average of measurements performed on three different samples (five measurements per sample), using distilled water droplets of 2 μL (glass slides) and 5 μL (foam samples).

3.1 Photocatalytic experiments

The photocatalytic properties of the plasma-coated samples were studied by evaluating their ability to degrade methyl orange in aqueous solution under UV irradiation. The experiments were carried out by using a small recirculating batch photoreactor purposely designed for the present study (Fig. 2). The experimental apparatus runs under controlled flow and irradiance conditions, and specifically consists of a Plexiglass photocatalytic cell connected to a peristaltic pump and an optical detector. The photocatalytic cell presents a cylindrical compartment (22 mm diameter, 4 mm height) where the photocatalytic materials to test (i.e., glass slides and PU foam samples) were placed. A quartz window (22 mm diameter) was located on the top of the cylindrical compartment, to close the photocatalytic cell and allow the UV irradiation of the sample. It is worth specifying that the volume of the photocatalytic cell (V_{cell} □ 1.5 mL) was

about 40% of the total volume of the experimental set-up (V_{tot} ≈ 3.6 mL). To favor the contact between the photocatalytic material and the recirculating methyl orange solution, the latter was introduced in the cell through four thin slits and forced to exit through other four slits located on the opposite side (Fig. 2). The solution flowed on the surface of the glass slides and through the porous structure of the foam samples (Fig. S2) at a constant flow rate of 50 ml·min^{-1}, as regulated by the peristaltic pump. UV irradiation was provided by a Vilbert Lourmat lamp (model VL-330) emitting in the 300-400 nm spectral range (maximum at 365 nm), and irradiance was kept fixed at 38 W_{UV}·m^{-2}. In each photocatalytic experiment (hereafter, also referred to as photocatalytic reaction run or cycle), the cell containing the plasma-coated samples was irradiated for 120 min to treat 3.6 ± 0.1 mL of a 10 mg·L^{-1} MO solution under recirculating flow conditions. The change in concentration of MO in the aqueous solution was followed by monitoring the MO UV-vis absorption spectra as a function of time. Spectra were acquired in-line every 10 min using an Avantes Optical spectrometer. Before starting the UV irradiation and absorbance measurements, the sample was placed in the photocatalytic cell, the target solution was introduced through the connector and allowed to flow in the closed circuit for 15 min under dark conditions. For each experiment, the recorded spectra were baseline corrected, smoothed and normalized using the Matlab software. Then, for each spectrum, the maximum absorbance value was extracted (in the wavelength range 420-464 nm) and the MO concentration was determined.

3. RESULTS AND DISCUSSION

3.1 Material characterization

Table 1 summarizes the processing conditions used in this work for the aerosol-assisted plasma deposition of TiO_2-containing nanocomposite coatings on the selected supporting substrates, i.e., the flat glass slides (Fig. 1b) and 3D porous PU foam samples (Fig. 1c). In particular, the

influence of the deposition time and of the oleate-capped TiO_2 NPs concentration in the starting dispersion was investigated, keeping fixed the electrical conditions used for DBD generation as well as the helium and dispersion flow rates.

Plasma processes were first carried out using the flat supporting samples which, among others, can facilitate the investigation of the structural and morphological properties of the nanocomposite coatings. In particular, the TiO_2-containing thin films were deposited on the glass slides from a 3 wt% oleate-capped TiO_2 NPs dispersion in a n-octane/1,7-octadiene mixture, by increasing the deposition time from 10 to 60 min (Table 1). Fig. 3 provides an overview of results from the ATR-FTIR, XPS and SEM characterization. The representative ATR-FTIR spectrum (Fig. 3a) shows the characteristic absorption bands associated with both the oleate-capped TiO_2 NPs and the hydrocarbon polymer formed by plasma polymerization of n-octane and 1,7-octadiene (Fig. S3) [54,57]. In particular, the spectrum displays the intense absorption band due to the Ti-O stretching vibrations (maximum at about 420 cm^{-1}) [58] and the oleate COO asymmetric and symmetric stretching signals (1300-1600 cm^{-1}) ascribed to the oleate-capped TiO_2 NPs (Fig. S3) [58–59]. Moreover, the typical absorption features of a plasma-deposited hydrocarbon polymer layer are also present, i.e., the CH_2 and CH_3 stretching and bending signals in the 2800-3000 cm^{-1} and 1300-1600 cm^{-1} regions, respectively (Fig. S3) [53,54,57]. It was found that the increase of the deposition time does not produce appreciable changes in the intensity ratio between the TiO_2 and the CH_x FTIR absorption bands and, therefore, in the chemical composition of the hybrid layers.

XPS analyses revealed that the surface atomic concentrations of carbon, oxygen and titanium are about 87, 10 and 3%, respectively, and remain invariant with the deposition time (Table S1). Fig. 3b presents the high-resolution XPS C 1s, O 1s and Ti 2p spectra of the NC coating deposited on a glass slide from a 3 wt% NPs dispersion for 60 min. The C 1s spectrum is dominated by the hydrocarbon component (284.8 ± 0.2 eV, 96%) and presents a very weak peak due to C-O groups (288.5 ± 0.2 eV, 4%). The high-resolution O 1s signal can be curve-

fitted with two peaks that can be ascribed to lattice oxygen in TiO_2 (529.7 ± 0.2, 76%) and to oxygen in OH, C-O and COO groups (531.9 ± 0.2, 24%) [60,61]. The position (464.2 ± 0.2 eV and 458.6 eV ± 0.2 eV) and separation (5.6 eV) of the Ti $2p_{1/2}$ and Ti $2p_{3/2}$ signals are in agreement with previous literature on anatase-rutile TiO_2 [60,61]. XRD investigation pointed out that TiO_2 NPs crystallinity was not affected by the deposition process, since both anatase and rutile typical reflections were observed in the diffraction patterns of the NC coating and of the pristine and oleate-capped P25 TiO_2 NPs (Fig. S4) [55].

SEM images in Figs. 3c and S5a reveal the deposition of hierarchical micro/nanostructured thin films. In particular, as already reported in the literature on the aerosol-assisted plasma deposition from NPs dispersions [43,53,54,57], the NC coatings consist of quasi-spherical NPs agglomerates coated by a thin polymeric layer (Figs. 3c and S5a). NPs agglomerates have mean size of about 700 nm (minimum and maximum size of ca. 100 and 2000 nm, respectively) and nearly log-normal size distribution with geometric standard deviation (σ_G) of about 1.6 (Fig. S6). The obtained distribution is in good agreement with typical size distributions of polydisperse aerosols produced with pneumatic atomizers [53]. The morphological features of the NC coatings well correlate with the above described XPS results and, specifically, with the fact that the surface chemical composition is dominated by the hydrocarbon polymer [43,53,54,57]. Interestingly, the organic component seems to play a twofold role: holding together the NPs agglomerates in the 3D network of the nanocomposite and ensuring the adhesion of the hybrid layer to the supporting substrate (Fig. S5a). The coexistence of a hierarchical multiscale surface texture and of the low surface energy hydrocarbon polymer explains the superhydrophobic behavior of the coatings which exhibit a water contact angle greater than 150° [43,53,54,57].

As estimated by the cross-sectional SEM observations (Fig. S5b), the maximum thickness of the thin films is 3.8 ± 0.5 μm, 6.7 ± 0.5 μm and 12.8 ± 1.0 μm for deposition times of 10, 30 and 60 min, respectively. In agreement with this trend, by increasing t_d from 10 to 60 min, the

weight of the coating deposited on the selected glass slides increases from 300 ± 30 to 2100 ± 300 μg, and the coating surface density increases from 0.79 ± 0.08 to 5.5 ± 0.8 $\mu g \cdot mm^{-2}$ (Table 1). Hence, it can be concluded that, under the investigated process condition, the mass deposition rate of the NC coating is about $9 \cdot 10^{-2}$ $\mu g \cdot mm^{-2} \cdot min^{-1}$.

Considering that the aim of the present work is to explore the use of the plasma-coated samples as photocatalytic materials for polluted water treatment, preliminary investigations were carried out to assess their stability upon water immersion for 24 h. Negligible changes were observed in the chemical composition, morphology and wettability of the NC films after water immersion, as assessed by ATR-FTIR, XPS and SEM as well as by WCA measurements. It is worth specifying that additional experiments were carried out to deposit NC coatings from more concentrated NPs dispersions (i.e., 5 wt%) with the objective of increasing the amount of NC coating deposited per sample as well as its overall mass deposition rate [54]. However, the thus-obtained plasma-coated samples underwent severe NPs detachment and coating delamination during water immersion. This drawback precluded their use in the photocatalytic tests.

Thin film deposition on the PU foam samples was investigated at two different deposition times (i.e., 30 and 60 min), by increasing the NPs concentration in the starting dispersion from 3 to 8 wt% (Table 1). Overall, it was found that the explored conditions allow varying the weight of the coating deposited per sample from 650 ± 60 to 2300 ± 300 μg and the coating surface density from 0.077 ± 0.007 to 0.27 ± 0.04 $\mu g \cdot mm^{-2}$ (Table 1). In particular, the mass deposition rate of the coating increases linearly from ~$2.6 \cdot 10^{-3}$ to ~$4.5 \cdot 10^{-3}$ $\mu g \cdot mm^{-2} \cdot min^{-1}$ by increasing the NPs concentration in the starting dispersion from 3 to 8 wt%.

XPS and SEM investigations were carried out to assess the uniformity of the NC coating over the entire 3D porous structure of the foam samples as well as to compare results obtained under different processing conditions. Table 2 reports the XPS surface atomic concentrations of the inner (i.e., cross section) and outer (i.e., top side) surfaces of all samples prepared in this work. It is worth specifying that XPS analyses were carried out on both the top and bottom sides of

the foam samples, however, since these two sides exhibited very similar surface composition, Table 2 only displays the surface atomic percentages of the sample top. In case of the pristine foam, XPS analyses revealed the presence of carbon, oxygen, nitrogen and silicon at atomic concentrations of about 74, 20.5, 4.5 and 1%, respectively. After plasma deposition, it was possible to observe the remarkable increase of the C atomic percentage, the decrease of the O atomic concentration, the appearance of Ti, and the disappearance of N and Si contributions from the pristine sample (Table 2). Moreover, Table 2 shows that with increasing the NPs concentration in the starting dispersion, the surface atomic concentrations of Ti and O increase, while the C atomic percentage decreases (Table 2). On the other hand, as also observed for the plasma-coated flat samples, the surface chemistry does not vary appreciably with deposition time, keeping fixed NPs concentration in the starting dispersion. It can also be appreciated that generally the cross-section and top side of the samples exhibit very similar XPS atomic percentages, revealing remarkable uniformity in surface composition. However, when deposition processes are carried out using an 8 wt% NPs dispersion, the Ti and O atomic percentages appear to be greater on the sample top than on the cross-section. As expected, the high-resolution XPS C1s, O 1s and Ti 2p spectra of the plasma-coated foam samples (Fig. 4a) are very similar to those observed for NC thin films deposited on the flat glass slides (Fig. 3b). It is worth noting that the typical C 1s spectrum of a plasma-coated foam presents only two components ascribed to aliphatic carbon and C-O moieties (Fig. 4a, Table S2); in contrast, the pristine foam is characterized by a very different C 1s lineshape (Fig. S7) that can be curve-fitted with four peaks centered at 284.8 ± 0.2 eV (C-C/C-H, 60%), 285.6 ± 0.2 eV (C-N, 5.5%), 286.4 ± 0.2 eV (C-O, 26.5%), 288.8 ± 0.2 eV (N-COO/COO, 8%) [45,47].

Fig. 5 displays representative SEM images of the pristine and plasma-coated foams. First of all, the low-magnification images (Figs. 5a,b) demonstrate that plasma ignition into the foam interior does not alter its porous structure. On the other hand, the high-magnification images (Figs. 5c-f) clearly evidence that the deposition strategy optimized in this work leads to the

complete coverage of the foam surfaces with the micro/nanostructured NC film. Overall, the plasma process enables the transition from the smooth surface of the pristine foam to the rough surface of the hydrocarbon polymer/TiO_2 NPs NC coating. In addition, as it can be appreciated in Fig. 6, the coverage level of the substrate and the surface density of the quasi-spherical NPs agglomerates immobilized on the foam surfaces increase with increasing both the deposition time and the oleate-capped TiO_2 NPs concentration in the starting dispersion. SEM observation of cross-sectioned ligaments of the plasma-coated foam allows roughly estimating the thickness of the NC coatings. For instance, Fig. 5f shows that the NC coating deposited on the foam sample for 60 min using a 3 wt% oleate-capped NPs dispersion has a maximum thickness of a few μm, considerably smaller than the one obtained on the glass slide under identical processing conditions (Fig. 3c). In agreement, Table 1 allows appreciating that, using a 3 wt% oleate-capped NPs dispersion and a deposition time of 60 min, the surface density of the coating on the glass slide (5.5 $\mu g \cdot mm^{-2}$) is about 35 times greater than that on the foam sample (0.155 $\mu g \cdot mm^{-2}$). This can be attributed to the combination of two factors: (i) the PU foam support has a surface area considerably larger than the glass slide (~22 times), (ii) the weight of the deposited coating is greater on the flat substrate than on the porous sample (~1.5 times) under the same plasma processing conditions (Table 1). This difference in coating weight could be explained considering that, when the foam is located in the DBD cell, the discharge develops in a series of volumes smaller than the total gas gap. This could reduce the gas bulk ionization degree. This effect could be further enhanced by the fact that the PU foam is made of an insulating material that is charged by the electrons or ions, reducing the local electric field. Thus, the field distribution is different in the foam and the gas ionization is probably lower, leading to a lower electron density. The observed phenomenon could be therefore explained as follows: in case of the foam, a lower density of electrons induces both (i) lower NPs charging and thus reduced transfer of the NPs to the foam surface [42,53] and (ii) lower dissociation of the organic precursors and thus reduced polymerization. At this stage this is a hypothesis. A

dedicated study is needed to clearly explain the lower coating weight and growth rate on the foam samples.

As observed for the glass slides, also the foam samples exhibited a superhydrophobic wetting behavior after thin film deposition (WCA > 150°). Interestingly, all plasma-coated porous samples prepared in this work showed remarkable chemical and morphological stability upon water immersion and were, therefore, tested in photocatalysis.

3.2 Photocatalytic performance

The photocatalytic activity of the plasma-coated samples listed in Table 1 was evaluated by the degradation of methyl orange in aqueous solution under UV light irradiation.

The mechanisms that lead to the photodegradation of molecules involve multiple processes such as charge generation, charge transfer, oxidation-reduction reactions on the catalyst surface, radical reaction. Many empirical laws have been proposed to describe these phenomena and to develop more or less advanced formalisms depending on the subject addressed [62,63]. When the objective is simply to evaluate or compare the photocatalytic ability of different materials [64,65], it is commonly acknowledged that the entire photodegradation process can be approximately described by a pseudo first-order kinetic model. In particular, taking into consideration the recirculating batch photoreactor used in this work, the photodegradation kinetics can be described by Eq. (1):

$$\frac{V_{cell}}{V_{tot}} \cdot \frac{dC(t)}{dt} = -\alpha \cdot I \cdot S \cdot C(t) \qquad (1).$$

where C is the concentration of the target molecule ($kg \cdot m^{-3}$), α is the energy constant ($s \cdot J^{-1}$), S is the irradiation area of the cell (m^2) and I is the flux density ($W \cdot m^{-2}$). From Eq. (1), it is possible to obtain the following expression for the concentration:

$$C(t) = C_0 \cdot \exp\left[-(\alpha \cdot I \cdot S) \cdot \left(\frac{V_{cell}}{V_{tot}} \cdot t\right)\right] \qquad (2).$$

where C_0 is the initial concentration.

Since in this work experimental data were obtained under constant irradiation conditions and for the same cell irradiation area, it is possible to introduce the apparent kinetic constant (k_{app}):

$$k_{app} = \alpha \cdot I \cdot S \qquad (3).$$

In addition, as reported in the literature [65], when a recirculating photoreactor is used, it is more appropriate to report the photodegradation kinetics as a function of the effective irradiation time (t_{irr}), which corresponds to the residence time of the MO solution in the photocatalytic cell. The effective irradiation time depends on the ratio between the cell volume and the total volume of experimental set-up, and can be calculated from Eq. (4):

$$t_{irr} = t \cdot \frac{V_{cell}}{V_{tot}} \qquad (4).$$

Eq. (2) can be therefore rewritten as:

$$C(t_{irr}) = C_0 \cdot \exp[- k_{app} \cdot t_{irr}] \qquad (5)$$

By determining the apparent kinetic constant of MO photodegradation using the different plasma-coated samples (Table 1), it is possible to compare (i) the photocatalytic activity of samples produced under different deposition conditions, in order to find the optimal preparation parameters, and (ii) the photocatalytic performance obtained with the two different supporting substrates, in order to highlight the potential benefits of using macroporous supports rather than conventional flat ones.

Figs. 7a,b display the evolution of the MO residual concentration ratio C/C_0 as a function of the effective irradiation time (where C_0 is the initial MO concentration and C the MO concentration at effective irradiation time t_{irr}) using two different plasma-coated samples: (i) a glass slide plasma-processed for 60 min using a 3 wt% NPs dispersion (Fig. 7a) and (ii) a foam sample processed for 60 min using an 8 wt% NPs dispersion (Fig. 7b). In particular, for both plasma-coated samples results from different consecutive reaction runs (i.e., cycles of use) are reported (runs 1, 3, 5, 20) along with methyl orange C/C_0 profiles obtained during blank experiments performed using the untreated samples (i.e., no TiO_2-containing coating) under both UV irradiation and dark conditions. First of all, results from blank experiments

demonstrate that negligible or moderate changes in MO concentration occur when the untreated samples are used. Secondly, Figs. 7a,b allow appreciating an evolution of the photocatalytic efficiency of the plasma-coated samples over the first three reaction runs. In particular, the first and second runs are characterized by slower photodegradation kinetics compared to the third one (Figs. 7a,b). It seems therefore that conditioning of the photocatalytic materials is needed to attain the best photocatalytic performance (i.e., two photocatalytic runs). The maximum photocatalyst efficiency is therefore reached at the 3rd run. Then, it remains unchanged for various consecutive runs (Figs. 7a,b show for instance the C/C_0 profiles for the 5th run). It is worthy to note that an analogous evolution of the photocatalytic efficiency was observed for all plasma-coated materials prepared in this work (Table 1).

To evaluate the influence of the supporting substrate and of the plasma deposition conditions on the photocatalytic activity, all plasma-coated samples were compared by determining the apparent kinetic constant for MO photocatalytic degradation at the 3rd cycle of use (Fig. 8). As far as the flat samples are concerned, results reveal that by increasing the DBD process duration from 10 to 60 min, i.e., by increasing both the thickness and weight of the deposited coatings, the apparent kinetic constant (and thus the catalytic efficiency) increases. The slight improvement in k_{app} value observed when t_d is increased from 30 to 60 min seems to point out that a plateau is reached. Various kinetic studies demonstrated that the photodegradation efficiency of TiO_2-based thin films increases with the film thickness up to a threshold value, above which the catalytic performance stabilizes [66,67]. This trend can be explained considering that, in principle, with increasing the coating thickness, the amount of photocatalyst available for reaction increases and, thus, the photodegradation performance is improved. However, when the thickness becomes too high, two phenomena could prevent the further increase of the photocatalytic efficiency: transfer limitation and UV light attenuation. It is in fact acknowledged that slow diffusion could limit the number of target molecules reaching the

interior of thick catalytic layers. Moreover, strong UV light attenuation could considerably reduce light penetration through the entire layer thickness.

Fig. 8 shows also that, in case of the foam samples, by increasing both the deposition time and NPs concentration in the starting dispersion, the apparent kinetic constant for MO degradation increases and, therefore, the photocatalytic efficiency increases. Overall, with the foam samples it is possible to achieve greater values of k_{app} than with the flat ones (Fig. 8).

It is difficult to compare the results obtained using the flat and macroporous samples. The photocatalytic performances can be compared, for instance, on the basis of two different criteria:

- If samples prepared under the same deposition condition are considered (i.e., 3 wt% NPs dispersion, 60 min), it can be observed that the apparent kinetic constant obtained with the flat support (□0.045 min^{-1}) is significantly higher than with the macroporous one (□0.035 min^{-1}). This is likely due to the remarkably greater amount of photocatalytic coating deposited on the flat support (Table 1). On the basis of this evidence, it could be concluded that, if the deposition conditions are kept fixed, the use of flat supports allows achieving superior photocatalytic activity. However, in this work, it was found that a narrow range of deposition conditions can be employed for the flat glass slides. For instance, as shown in the previous section, when dispersions with NPs concentration greater than 3 wt% were used, the plasma-coated glass slides were unstable in water and cannot be tested in photocatalytic experiments. In contrast, in the case of the foam supports, it was possible to increase the NPs concentration, eventually reaching greater values of k_{app} as compared to the flat slides (Fig. 8).
- If samples coated with similar amounts of photocatalytic film are considered, it can be observed that the macroporous samples are more efficient than the flat ones. This can be appreciated, for instance, by comparing the best-performing flat sample (resulting from plasma deposition for 60 min using a 3 wt% NPs dispersion) and the best-performing foam

sample (resulting from plasma deposition for 60 min using an 8 wt% NPs dispersion), which are loaded with very similar amounts of photocatalytic coating (i.e., 2100 ± 300 μg and 2300 ± 300 μg, respectively, Table 1). Fig. 8 clearly shows that the k_{app} of the foam sample is □0.09 min^{-1} and, thus, significantly greater than that of the flat sample (□0.045 min^{-1}). This finding points to the benefits of using macroporous supports for photocatalyst immobilization. Macroporous supports allow obtaining a high active surface area per unit of photoreactor volume [22-31,38], with two main advantages as compared with conventional flat supports: (i) the first is that the photooxidation rate is greater because of the larger surface area available for light capture; (ii) the second is that mass transfer limitations are minimized because the effective surface area available for reaction is larger.

For the above mentioned best-performing flat and macroporous samples, recyclability was evaluated over 20 cycles of use, which correspond to a total operation time in photocatalysis of 40 h. It was found that the plasma-coated glass slide maintains high photocatalytic activity after prolonged use, without appreciable loss of efficiency. After twenty cycles of use, negligible changes were observed in methyl orange C/C_0 profile (Fig. 7a) and, consequently, in k_{app} (~0.045 min^{-1}). In contrast, the plasma-coated foam sample starts to lose efficiency after seven photocatalytic cycles. Fig. 7b reports the MO C/C_0 profile of the 20th reaction run, from which it was possible to obtain that the k_{app} for MO degradation is ~0.04 min^{-1}, less than half that of the 3rd run. To compare the reusability of the best-performing flat and porous samples, Fig. 7c reports the MO removal determined for each reaction run at the 75% of the total run duration. Specifically, the MO removal was calculated as the percentage ratio between the MO amount removed at the 75% of the run duration and the initial MO amount. In case of the plasma-coated glass slide MO removal reaches ~85% at the 3rd run and remains unchanged even after 20 consecutive runs. On the other hand, in case of the foam sample, the MO removal is almost complete (~95-100%) for the runs from 2 to 9, then it slightly decreases to 85% after 20 runs.

It can be thus concluded that both samples present remarkable reusability and maintained good activity after prolonged operation (40 h).

3.3 Evolution of the plasma-coated samples upon use in photocatalytic water treatment

To gain insights into the evolution of the photocatalytic activity of the plasma-coated materials over multiple reaction runs, the chemical composition, morphology and wettability of the best-performing glass slide (i.e., plasma-coated in a DBD for 60 min using a 3 wt% NPs dispersion) and PU foam sample (i.e., plasma-coated in a DBD for 60 min using an 8 wt% NPs dispersion) was investigated as a function of the operation time in photocatalytic water treatment. Specifically, XPS analyses, SEM observations, and WCA measurements were performed on:

(i) the as deposited samples;

(ii) the plasma-coated samples after two photocatalytic reaction runs (i.e., after 4 h of operation under UV light irradiation), considering that, as previously shown, two runs seem to be needed to obtain the maximum photocatalytic performance (Figs. 7a,b);

(iii) the plasma-coated samples, after twenty photocatalytic reaction runs, i.e., after 40 h of operation under UV light irradiation.

It is relevant to remark that published studies reporting on the recyclability of novel immobilized photocatalysts are very rarely accompanied by a detailed characterization of the photocatalytic materials after use in wastewater treatment.

In case of the best-performing flat sample, XPS results reported in Table 3 show that, by increasing the photocatalyst operation time from 0 to 4 h, a remarkable decrease of the C surface atomic concentration is observed (from 87% to 56%), along with a concomitant increase of the Ti and O percentages from 3% to 11% and from 10% to 33%, respectively. This variation in surface chemical composition can be ascribed to the partial degradation of the organic component of the NC by strong oxidants formed at the TiO_2 NPs surface during the photocatalytic reaction, as reported in the literature on the use of organic polymer/TiO_2

composites for photocatalytic water treatment [5,68,69]. The partial degradation of the hydrocarbon polymer leads to a greater exposure of the TiO_2 NPs immobilized on the sample surface (increase of the Ti atomic surface concentration, Table 3) and could explain the typical enhancement of the photocatalytic performance observed over the first three cycles of reaction (Fig. 7a). By prolonging the catalyst operation up to 40 h, the C surface atomic concentration further decreases down to 30%, while the Ti and O percentages increase up to 19% and 51%, respectively. However, this further change in the surface composition seems not to lead to new variations in the photocatalytic activity that remains stable from the 3rd to the 20th reaction run (Fig. 7a,c).

Table 4 and Fig. S8 clearly show that, after use in photocatalysis, the high-resolution XPS C 1s spectrum of the plasma-coated flat sample displays new contributions from oxygen-containing functionalities formed through polymer oxidation. The C 1s spectrum can be, in fact, curve-fitted with four components ascribed to C-C/C-H (284.8 ± 0.2 eV), C-O (286.4 ± 0.2 eV), C=O/O-C-O (287.4 ± 0.2 eV) and COO (288.5 ± 0.2 eV) functional groups (Table 4 and Fig. S8). Interestingly, the peak area percentage of the C 1s aliphatic component, which is equal to 96% for the as-deposited flat sample, decreases to about 80% after 2 and 20 reaction runs. On the other hand, the percentages of the components due to oxygen-containing functionalities increase. For instance, the peak area percentage of the COO component (288.5 ± 0.2 eV) increases up to 8% after 20 runs. The high-resolution XPS O 1s signal can be curve-fitted with two components ascribed to oxygen in TiO_2 and to oxygen in COO, OH and C-O groups (Fig. S8). Fig. S8 shows that the O 1s lineshape changes slightly after 2 reaction runs, while after 20 runs it appears to be very similar to that of the TiO_2 nanoparticles (not shown). Finally, no appreciable changes in the Ti 2p spectrum were observed after sample use in photocatalysis (Fig. S8).

Cross-sectional SEM images of the plasma-coated glass slide in Fig. 9 reveal that after 2 cycles of reaction a certain reorganization of the nanocomposite occurs (i.e., the NPs agglomerates

seems to be more densely packed in the NC) along with a moderate reduction in coating thickness (Fig. 9c). This reduction becomes more evident after 20 runs. However, it is worth highlighting that after prolonged use in photocatalysis (20 runs), both the NPs agglomerates and the organic component are still visible in the coating (Fig. 9e and Fig. S9), whose thickness remains as high as 8.2 ± 0.8 μm. Overall, after 20 reaction runs a thickness and weight loss of □40% was detected. These evidences, in conjunction with results from XPS analyses, could explain why the photocatalytic performance of the plasma-coated glass slide remains stable also after 20 reaction runs (Fig.7a,c). The reduction of the coating thickness and weight upon photocatalytic reaction could be due to the following causes: (i) the photocatalytic reaction itself that can induce the degradation of the organic component [5,68,69], leading to NPs release in water and reorganization of the NPs agglomerates in the coating; (ii) the mechanical stress due to MO solution flow in the recirculating reactor (Fig. S2a), that could cause for instance NPs detachment. It is worth noting that, considering the coating weight loss detected after 20 reaction cycles, the maximum expected concentration of TiO_2 in the treated solution is □12 mg/L. This concentration is in the range of the nanoscale TiO_2 toxicity thresholds currently reported for aquatic organisms (threshold limits generally > 10 – 100 mg/L) [70,71]. Efforts should be directed towards the improvement of the chemical durability of the deposited coatings varying, for instance, the nature of the nanocomposite matrix (e.g., inorganic silica-like matrix, organosilicon and/or fluorocarbon polymeric matrix).

Further observations can be made regarding the evolution of the sample wettability. The as-deposited glass slide was superhydrophobic and, in fact, exhibited a WCA of 160 ± 3° (Table 3) [57,72]. The WCA value decreased to 140 ± 3° after 2 reaction runs and to less than 5° after 20 runs (i.e., superhydrophilic character). The WCA decrease is, first of all, a consequence of changes in the surface chemical composition of the sample (XPS data in Tables 3 and 4) which is due, for instance, to the oxidation of the low-surface energy polymeric component of the NC. On the other hand, the fact that a superhydrophilic surface is obtained after prolonged use in

photocatalysis (40 h operation) could also be ascribed to phenomena involving the interaction between the UV light and TiO_2 NPs surface [73,74].

An analogous study was carried out for the best-performing foam sample resulting from a 60 min plasma deposition with an 8 wt% TiO_2 NPs dispersion. XPS results show that, with increasing the operation time in photocatalysis from 0 to 4 h, the C atomic concentration decreases, while the O and Ti percentages increase both on the exterior and interior surfaces of the porous sample (Table 5). However, further increasing the operation time up to 40 h leads to a slight decrease of the Ti percentages (8 and 3% for the sample top and cross-section, respectively) with respect to the sample after 4 h of operation (10 and 4% for the sample top and cross-section, respectively). This decrease, in conjunction with the appearance of the nitrogen contribution ascribed to the pristine PU foam (Table 5), indicates the loss of a certain amount of TiO_2 NPs and suggests that the coating thickness could be at some points smaller than the sampling depth of XPS (~10 nm). As shown in Fig. 4 and Table S2, after use in photocatalysis, the high-resolution XPS C 1s spectrum of the foam displays more intense contributions ascribed to oxygen-containing functionalities (as observed for the flat samples). Interestingly, after 20 reaction cycles, the appearance of the C-N component due to the polyurethane foam (N-COO functionalities) is observed suggesting a decrease in film thickness. A remarkable change of O 1s spectrum can be also detected (Figure 4), due to the increased contribution of the component ascribed to OH, C-O and COO groups (531.5 ± 0.2 eV) [60,61]. On the other hand, the shape and position of the Ti 2p signal does not appreciably change after sample use in photocatalysis (Fig. 4).

The SEM images taken in the interior of the plasma-coated foam confirm the decrease of the NC coating thickness and of the NPs agglomerates surface density upon use in photocatalysis (Fig. 9). This evidence, together with XPS data, can justify the partial loss of the photocatalytic efficiency over 20 reaction runs (Fig. 7b,c).

The use of the foam sample in photocatalysis determines the decrease of the WCA from 135 ± 5° to 80 ± 20° after 20 reaction runs (Table 5). The WCA decrease can be reasonably ascribed to the variation of the surface composition of the sample and in particular to the partial degradation of the hydrocarbon polymer present in the NC coating. It is worth specifying that the WCA of the pristine foam is 102 ± 5°.

Overall, the evolution of the best-performing foam sample upon use in photocatalysis is very similar to that of the best-performing glass slide. The foam sample maintains remarkable photocatalytic performance also after 20 reaction runs (Figs. 7b,c). However, a decrease in the apparent kinetic constant for MO degradation is detected after prolonged use (Figs. 7b). This could be mainly ascribed to decrease of the coating thickness and to partial loss of TiO_2 NPs as a function of the operation time in photocatalysis (Figs. 9b,d,f).

4. CONCLUSION

In this work, an aerosol-assisted atmospheric pressure plasma process was used to deposit photocatalytic hydrocarbon polymer/TiO_2 nanoparticles NC coatings onto different supporting substrates, i.e., open-cell polyurethane foams and flat glass slides.

Plasma-coated materials prepared under different deposition conditions were characterized by XPS, ATR-FTIR, SEM and WCA measurements. Obtained results revealed the potential of the developed plasma process for the controlled deposition of TiO_2-based coatings on complex 3D macroporous substrates such as the PU foams. The photocatalytic activity of the plasma-coated samples was assessed by the degradation of methyl orange in aqueous solution under UV illumination, using a purposely designed recirculating batch photoreactor. The comparative study showed that greater photocatalytic activity can be achieved using as supporting substrates the PU foams rather than the glass slides. These findings confirmed the benefits of using macroporous supports for photocatalyst immobilization rather than conventional flat ones. The prepared photocatalytic materials presented remarkable reusability and maintained good

activity over 20 reaction runs, corresponding to 40 h of photocatalyst operation in wastewater treatment. However, while no changes in photocatalytic activity were observed in case of the best-performing plasma-coated glass slide, a slight loss in activity (decrease of k_{app}) was detected for the best-performing foam sample. This loss seemed to be mainly ascribed to decrease of the coating thickness and to partial detachment of TiO_2 NPs, as assessed through the detailed characterization of the surface chemical composition and morphology of the plasma-coated samples as a function of the operation time in photocatalytic water treatment. Future work will be directed towards the improvement of the durability of the deposited coatings by varying, for instance, the chemical nature of the nanocomposite film matrix.

ASSOCIATED CONTENT

Supporting Information

Atmospheric pressure DBD reactor and sample positioning; surface area of the supporting substrates; experimental details on XPS, ATR-FTIR and SEM analyses; photocatalytic cell schematics; ATR-FTIR spectra and XPS results of the oleate-capped TiO_2 NPs, of the hydrocarbon coating and of the NC coating; XRD diffractograms; additional SEM images of NC coatings deposited on the glass slides; NPs agglomerate size distribution in the NC coating; curve-fitting results of high-resolution XPS C 1s spectra of the best-performing plasma-coated foam before and after two and twenty photocatalytic runs; high-resolution XPS C 1s spectrum of the pristine foam; high resolution XPS C 1s, O 1s, Ti 2p spectra of the best-performing plasma-coated glass slide before and after two and twenty photocatalytic runs; additional SEM images of NC coatings deposited on the glass slides after photocatalysis.

Notes

The authors declare no competing financial interest.

ACKNOWLEDGEMENTS

The authors would like to gratefully acknowledge Prof. Francesco Fracassi (University of Bari 'Aldo Moro', Bari, Italy) for the many valuable discussions. Dr. Bernard Fraisse (University of Montpellier, France) is acknowledged for XRD analyses. Danilo Benedetti, Savino Cosmai and Teresa Lasalandra are also acknowledged for the technical assistance. This research was supported by the Italian Ministry for Education, University and Research (MIUR) under grant PONa3_00369 and ARS01_00849, and Regione Puglia under grant no. 51 "LIPP" (within the Framework Programme Agreement APQ "Ricerca Scientifica", II atto integrativo - Reti di Laboratori Pubblici di Ricerca). A.U. gratefully acknowledges MIUR for funding her PhD research fellowship (PON FSE-FESR Research and Innovation 2014-2020). This work was also supported by French 'Investments for the future' ('Investissements d'Avenir') programme managed by the National Agency for Research (ANR) under contract ANR10LABX2201 (labex SOLSTICE).

REFERENCES

[1] M.R. Hoffmann, S.T. Martin, W. Choi, D.W. Bahnemann, Environmental applications of semiconductor photocatalysis, Chem. Rev. 95 (1995) 69–96. https://doi.org/10.1021/cr00033a004

[2] S.K. Loeb, P.J.J. Alvarez, J.A. Brame, E.L. Cates, W. Choi, J. Crittenden, D.D. Dionysiou, Q. Li, G. Li-Puma, X. Quan, D.L. Sedlak, T.D. Waite, P. Westerhoff, J.-Ho. Kim, The technology horizon for photocatalytic water treatment: sunrise or sunset?, Environ. Sci. Technol. 53 (2019) 2937−2947. https://doi.org/10.1021/acs.est.8b05041

[3] S. Ahmed, M.G. Rasul, R. Brown, M.A. Hashib, Influence of parameters on the heterogeneous photocatalytic degradation of pesticides and phenolic contaminants in wastewater: A short review, J. Environ. Manag. 92 (2011) 311–330. https://doi.org/10.1016/j.jenvman.2010.08.028

[4] A.Y. Shan, T. Idaty, M. Ghazi, S.A. Rashid, Immobilisation of titanium dioxide onto Supporting Informations in heterogeneous photocatalysis: a review, Appl. Catal. A Gen. 389 (2010) 1–8. https://doi.org/10.1016/j.apcata.2010.08.053

[5] S. Singh, H. Mahalingam, P.K. Singh, Polymer-supported titanium dioxide photocatalysts for environmental remediation: A review, Appl. Catal. A Gen. 462–463 (2013) 178–195. https://doi.org/10.1016/j.apcata.2013.04.039

[6] V.K.H. Bui, V.V. Tran, J-Y Moon, D. Park, Titanium dioxide microscale and macroscale structures: a mini-review, Nanomaterials. 10 (2020) 1190. https://doi.org/10.3390/nano10061190

[7] R. Ghoutham, R. Badri Narayan, B. Srikanth, K.P. Gopinath, Supporting Informations for immobilisation of nano-photocatalysts, in: G. Sharma, A. Kumar, E. Lichtfouse, A. Asiri (Eds.), Nanophotocatalysis and Environmental Applications. Environmental Chemistry for a Sustainable World, Springer, Cham, 2019, pp. 49–82.

[8] J. Wang, S. Sun, H. Ding, W. Chen, Y. Liang, Preparation of a composite photocatalyst with enhanced photocatalytic activity: Smaller TiO_2 carried on SiO_2 microsphere, Appl. Surf. Sci. 493 (2019) 146–156. https://doi.org/10.1016/j.apsusc.2019.07.005

[9] S. Collette, J. Hubert, A. Batan, K. Baert, M. Raes, I. Vandendael, A. Daniel, C. Archambeau, H. Terryn, F. Reniers, Photocatalytic TiO_2 thin films synthesized by the post-discharge of an RF atmospheric plasma torch, Surf. Coat. Technol. 289 (2016) 172–178. https://doi.org/10.1016/j.surfcoat.2016.01.049

[10] C. da Trindade, S.W. Da Silva, Synthesis and characterization of TiO_2 films onto AISI 304 metallic meshes and their application in the decomposition of the endocrine-disrupting alkylphenolic chemicals, Appl. Surf. Sci. 457 (2018) 644–654. https://doi.org/10.1016/j.apsusc.2018.06.287

[11] Y.-Y. Wei, X.-T. Sun, Z.-R. Xu, One-step synthesis of bifunctional PEGDA/TiO_2 composite film by photopolymerization for the removal of Congo red, Appl. Surf. Sci. 445 (2018) 437–444. https://doi.org/10.1016/j.apsusc.2018.03.149

[12] S.D. Tigno, M.U. Herrera, M.D.L. Balela, Hydrophobicity of functionalized TiO_2-based kapok nanocomposite, Surf. Coat. Technol. 350 (2018) 857–862. https://doi.org/10.1016/j.surfcoat.2018.04.017

[13] N. Vodisek, A. Suligoj, D. Korte, U.L. Stangar, Transparent photocatalytic thin films on flexible polymer substrates, Materials. 11 (2018) 1945. https://dx.doi.org/10.3390%2Fma11101945

[14] A. Perraundeau, C. Dublanche-Tixier, P. Tristanct, C. Chazelas, Dynamic mode optimization for the deposition of homogeneous TiO_2 thin film by atmospheric pressure PECVD using microwave plasma torch, Appl. Surf. Sci. 493 (2019) 703–709. https://doi.org/10.1016/j.apsusc.2019.07.057

[15] S. Krumdieck, R. Gorthy, A.J. Gardecka, D. Lee, S.S. Miya, S.D. Talwar, M.I.J. Polson, C. Bishop, Characterization of photocatalytic, wetting and optical properties of TiO_2 thin films and demonstration of uniform coating on 3-D surface in the mass transport controlled

regime, Surf. Coat. Technol. 326 (2017) 402–410. https://doi.org/10.1016/j.surfcoat.2016.11.064

[16] D. Li, N. Gautier, B. Dey, S. Bulou, M. Richard-Plouet, W. Ravisy, A. Goullet, P. Choquet, A. Granier, TEM analysis of photocatalytic TiO_2 thin films deposited on polymer substrates by low-temperature ICP-PECVD, Appl. Surf. Sci. 491 (2019) 116–122. https://doi.org/10.1016/j.apsusc.2019.06.045

[17] J. Yu, Z. Pang, C. Zheng, T. Zhou, J. Zhang, H. Zhou, Q. Wei, Cotton fabric finished by PANI/TiO_2 with multifunctions of conductivity, anti-ultraviolet and photocatalysis activity, Appl. Surf. Sci. 470 (2019) 84–90. https://doi.org/10.1016/j.apsusc.2018.11.112

[18] M. Cizmic, D. Ljubas, M. Rozman, D. Asperger, L. Curkovic, S. Babic, Photocatalytic degradation of azithromycin by nanostructured TiO_2 film: kinetic, degradation products, and toxicity, Materials. 12 (2019) 873. https://dx.doi.org/10.3390%2Fma12060873

[19] A. Vahl, S. Veziroglu, B. Henkel, T. Strunskus, O. Polonskyi, O. C. Aktas, F. Faupel, Pathway to tailor photocatalytic performance of TiO_2 thin films deposited by reactive magnetron sputtering, Materials. 12 (2019) 2840. https://doi.org/10.3390/ma12172840

[20] H. Guo, M. Kemell, M. Heikkila, M. Leskela, Noble metal-modified TiO_2 thin film photocatalyst on porous steel fiber support, Appl. Catal. B Environ. 95 (2010) 358–364. https://doi.org/10.1016/j.apcatb.2010.01.014

[21] M. Coto, S.C. Troughton, J. Duan, R.V. Kumar, T.W. Clyne, Development and assessment of photo-catalytic membranes for water purification using solar radiation, Appl. Surf. Sci. 433 (2018) 101–107. https://doi.org/10.1016/j.apsusc.2017.10.027

[22] K. Elatmani, N. Ben oujji, G. Plantard, V. Goetz, I. Ait ichou, 3D Photocatalytic media for decontamination of water from pesticides, Mater. Res. Bull. 101 (2018) 6–11. https://doi.org/10.1016/j.materresbull.2017.12.042

[23] I.J. Ochuma, O.O. Osibo, R.P. Fishwick, S. Pollington, A. Wagland, J. Wood, J.M. Winterbottom, Three-phase photocatalysis using suspended titania and titania supported on a reticulated foam monolith for water purification, Catal. Today 128 (2007) 100–107. https://doi.org/10.1016/j.cattod.2007.05.015

[24] G. Plesch, M. Gorbár, U.F. Vogt, K. Jesenák, M. Vargová, Reticulated macroporous ceramic foam supported TiO_2 for photocatalytic applications, Mater. Lett. 63 (2009) 461–463. https://doi.org/10.1016/j.matlet.2008.11.008

[25] S. Hajiesmanili, S. Josset, D. Begin, C. Pham-Huu, N. Keller, V. Keller, 3D solid carbon foam-based photocatalytic materials for vapor phase flow-through structured photoreactors, Appl. Cat. A. Gen. 382 (2010) 122–130. https://doi.org/10.1016/j.apcata.2010.04.044

[26] M. Vargová, G. Plesch, U.F. Vogt, M. Zahoran, M. Gorbár, K. Jesenák, TiO_2 thick films supported on reticulated macroporous Al_2O_3 foams and their photoactivity in phenol mineralization, Appl. Surf. Sci. 257 (2011) 4678–4684. https://doi.org/10.1016/j.apsusc.2010.12.121

[27] G. Plantard, F. Correia, V. Goetz, Kinetic and efficiency of TiO_2-coated on foam or tissue and TiO_2-suspension in a photocatalytic reactor applied to the degradation of the 2,4-dichlorophenol, J. Photochem. Photobiol. A Chem. 222 (2011) 111–116. https://doi.org/10.1016/j.jphotochem.2011.05.009

[28] G. Plantard, V. Goetz, Correlations between optical, specific surface and photocatalytic properties of media integrated in a photo-reactor, Chem. Eng. J. 252 (2014) 194–201. https://doi.org/10.1016/j.cej.2014.04.055

[29] S.W. da Silva, J.P. Bortolozzi, E.D. Banus, A.M. Bernardes, M.A. Ulla, TiO_2 thick films supported on stainless steel foams and their photoactivity in the nonyphenol ethoxylate mineralization, Chem. Eng. J. 283 (2016) 1264–1272. https://doi.org/10.1016/j.cej.2015.08.057

[30] I. Levchuk, C. Guillard, F. Dappozze, S. Parola, D. Leonard, M. Sillanpaa, Photocatalytic activity of TiO_2 films immobilized on aluminum foam by atomic layer deposition technique, J. Photochem. Photob. 328 (2016) 16–23. https://doi.org/10.1016/j.jphotochem.2016.03.034

[31] C. Wang, Z-H Shi, L. Peng, W He, B. Li, K Li, Preparation of carbon foam-loaded nano-TiO_2 photocatalyst and its degradation on methyl orange, Surf. Interf. 7 (2017) 116–124. https://doi.org/10.1016/j.surfin.2017.03.007

[32] M. Martín-Sómer, C. Pablos, A. de Diego, R. van Grieken, A. Encinas, V.M. Monsalvo, J. Marugan, Novel macroporous 3D photocatalytic foams for simultaneous wastewater disinfection and removal of contaminants of emerging concern, Chem. Eng. J. 366 (2019) 449–459. https://doi.org/10.1016/j.cej.2019.02.102

[33] Z. Svagelj, V. Mandic, L. Curkovic, M. Biosic, I. Zmak, M. Gaborardi, Titania-coated alumina foam photocatalyst for memantine degradation derived by replica method and sol-gel reaction, Materials. 13 (2020) 227. https://doi.org/10.3390/ma13010227

[34] T. Yildiz, H. G. Yatmaz, K. Ozturk, Anatase TiO_2 powder immobilized on reticulated Al_2O_3 ceramics as a photocatalyst for degradation of RO16 azo dye, Ceram. Int. 46 (2020) 8651–8657. https://doi.org/10.1016/j.ceramint.2019.12.098

[35] L. Zhang, Z. Xing, H. Zhang, Z. Li, X. Zhang, Y. Zhang, L. Li, W. Zhou, Multifunctional floating titania-coated macro/mesoporous photocatalyst for efficient contaminant removal, ChemPlusChem 80 (2015) 623–629. https://doi.org/10.1002/cplu.201402327

[36] L. Li, Y. Li, H. Xu, W. Zhang, Novel floating TiO_2 photocatalysts for polluted water decontamination based on polyurethane composite foam, Sep. Sci. Technol. 50 (2015) 164–173. https://doi.org/10.1080/01496395.2014.949773

[37] T. Liu, S. Sun, L. Zhou, P. Li, Z. Su, G. Wei, Polyurethane-supported graphene oxide foam functionalized with carbon dots and TiO_2 particles for photocatalytic degradation of dyes, Appl. Sci. 9 (2019) 293. https://doi.org/10.3390/app9020293

[38] T. Van Gerven, G. Mul, J. Moulijn, A. Stankiewicz, A review of intensification of photocatalytic processes, Chem. Eng. Process. 46 (2007) 781-789. https://doi.org/10.1016/j.cep.2007.05.012

[39] S. Banarjee, E. Adhikari, P. Sapkota, A. Sebastian, S. Ptasinska, Atmospheric pressure plasma deposition of TiO_2: a review, Materials. 13 (2020) 2931. https://doi.org/10.3390/ma13132931

[40] J. Profili, O. Levasseur, N. Naudé, C. Chaneac, L. Stafford, N. Gherardi, Influence of the voltage waveform during nanocomposite layer deposition by aerosol-assisted atmospheric pressure Townsend discharge, J. Appl. Phys. 120 (2016) 053302. https://doi.org/10.1063/1.4959994

[41] K. Baba, S. Bulou, P. Choquet, N. D. Boscher, Photocatalytic anatase TiO_2 thin films on polymer optical fiber using atmospheric-pressure plasma, ACS Appl. Mat. Inter. 9 (2017) 13733–13741. https://doi.org/10.1021/acsami.7b01398

[42] P. Brunet, R. Rincón, J.M. Martinez, Z. Matouk, F. Fanelli, M. Chaker, F. Massines, Control of composite thin film made in an Ar/isopropanol/TiO_2 nanoparticles dielectric barrier discharge by the excitation frequency, Plasma Process. Polym. 14 (2017) e1700049. https://doi.org/10.1002/ppap.201700049

[43] P. Brunet, R. Rincón, Z. Matouk, M. Chaker, F. Massines, Tailored waveform of dielectric barrier discharge to control composite thin film morphology, Langmuir 34 (2018) 1865–1872. https://doi.org/10.1021/acs.langmuir.7b03563

[44] G. Jnido, G. Ohms, W. Viol, One-step deposition of Polyester/TiO_2 coatings by atmospheric plasma jet on wood surfaces for UV and moisture protection, Coatings. 10 (2020) 184. https://doi.org/10.3390/coatings10020184

[45] F. Fanelli, F. Fracassi, Thin film deposition on open-cell foams by atmospheric pressure dielectric barrier discharges, Plasma Process. Polym. 13 (2016) 470–479. https://doi.org/10.1002/ppap.201500150

[46] F. Fanelli, P. Bosso, A.M. Mastrangelo, F. Fracassi, Thin film deposition at atmospheric pressure using dielectric barrier discharges: advances on three-dimensional porous substrates and functional coatings, Jpn. J. Appl. Phys. 55 (2016) 07LA01. https://doi.org/10.7567/JJAP.55.07LA01

[47] V. Armenise, A. Milella, F. Fracassi, P. Bosso, F. Fanelli, Deposition of thin films containing carboxylic acid groups on polyurethane foams by atmospheric pressure non-equilibrium plasma jet, Surf. Coat. Technol. 379 (2019) 125017. https://doi.org/10.1016/j.surfcoat.2019.125017

[48] M. Michlicek, A. Manakhov, E. Dvorakova, L. Zajickova, Homogeneity and penetration depth of atmospheric pressure plasma polymerization onto electrospun nanofibrous mats, Appl. Surf. Sci. 471 (2019) 835–841. https://doi.org/10.1016/j.apsusc.2018.11.148

[49] M. Michlicek, L. Blahová, E. Dvoraková, D. Necas, L. Zajicková, Deposition penetration depth and sticking probability in plasma polymerization of cyclopropylamine, Appl. Surf. Sci. 540 (2021) 147979. https://doi.org/10.1016/j.apsusc.2020.147979

[50] L.-F. Meunier, J. Profili, S. Babaei, S. Asadollahi, A. Sarkissian, A. Dorris, S. Beck, N. Naudé, L. Stafford, Modification of microfibrillated cellulosic foams in a dielectric barrier discharge at atmospheric pressure, Plasma Process. Polym. (2020) e2000158. https://doi.org/10.1002/ppap.202000158

[51] L. Cheng, R. Ghobeira, P. Cools, Z. Liu, K. Yan, N. De Geyter, R. Morent, Comparative study of different nitrogen-containing plasma modifications applied on 3D porous PCL scaffolds and 2D PCL films, Appl. Surf. Sci. 516 (2020) 146067. https://doi.org/10.1016/j.apsusc.2020.146067

[52] S. Wang, Y. Zhang, T. Zhang, F. Dong, H. Huang, Readily attainable spongy foam photocatalyst for promising practical photocatalysis, Appl. Catal. B Environ. 208 (2017) 75–81. https://doi.org/10.1016/j.apcatb.2017.02.033

[53] F. Fanelli, A.M. Mastrangelo, F. Fracassi, Aerosol-assisted atmospheric cold plasma deposition and characterization of superhydrophobic organic-inorganic nanocomposite thin films, Langmuir 30 (2014) 857–865. https://doi.org/10.1021/la404755n

[54] F. Fanelli, A.M. Mastrangelo, G. Caputo, F. Fracassi, Tuning the structure and wetting properties of organic-inorganic nanocomposite coatings prepared by aerosol-assisted atmospheric pressure cold plasma deposition, Surf. Coat. Technol. 358 (2019) 67–75. https://doi.org/10.1016/j.surfcoat.2018.11.020

[55] X. Yin, Z. Xue, L. Wang, Y. Cheng, B. Liu, High-Performance Plastic Dye-sensitized Solar Cells Based on Low-Cost Commercial P25 TiO_2 and Organic Dye, ACS Appl. Mater. Interfaces 4 (2012) 1709–1725. https://doi.org/10.1021/am201842n

[56] F. Topin, J.-P. Bonnet, B. Madani, L. Tradist, Experimental analysis of multiphase flow in metallic foam: convective boiling, flow laws and heat transfer, Adv. Eng. Mater. 8 (2006) 890-899. https://doi.org/10.1002/adem.200600102

[57] F. Fanelli, A.M. Mastrangelo, N. De Vietro, F. Fracassi, Preparation of multifunctional superhydrophobic nanocomposite coatings by aerosol-assisted atmospheric cold plasma deposition, Nanosci. Nanotechnol. Lett. 7 (2015) 84–88. https://doi.org/10.1166/nnl.2015.1943

[58] G. Caputo, R. Cingolani, P.D. Cozzoli, A. Athanassiou, Wettability conversion of colloidal TiO_2 nanocrystal thin films with UV-switchable hydrophilicity, Phys. Chem. Chem. Phys., 11 (2009) 3692–3700. https://doi.org/10.1039/B823331D

[59] G.B. Deacon, R.J. Phillips, Relationship between the carbon-oxygen stretching frequencies of carboxylato complexes and the type of carboxylate coordination, Coord. Chem. Rev. 33 (1980) 227–250. https://doi.org/10.1016/S0010-8545(00)80455-5

[60] B. Erdem, R.A. Hunsicker, G.W. Simmons, E.D. Sudol, V.L. Dimonie, M.S. El-aasser, XPS and FTIR Surface Characterization of TiO_2 Particles Used in Polymer Encapsulation, Langmuir. 17 (2001) 2664–2669. https://doi.org/10.1021/la0015213

[61] D. Barreca, TiO_2 Thin Films by Chemical Vapor Deposition: An XPS Characterization, Surf. Sci. Spectra. 14 (2007) 27-33. https://doi.org/10.1116/11.20070902 EX65

[62] A.V. Emeline, V. Ryabchuk, N. Serpone, Factors affecting the efficiency of a photocatalysed process in aqueous metal-oxide dispersions. Prospect of distinguishing between two kinetic models, J. Photochem. Photobiol. A, 133 (2000) 89–97. https://doi.org/10.1016/S1010-6030(00)00225-2

[63] G. Plantard, and V. Goetz, Experimental and numerical studies of a solar photocatalytic process in a dynamic mode applied to three catalyst media, Chem. Eng. Process. 62 (2012) 129-136. https://doi.org/10.1016/j.cep.2012.08.002

[64] K. Elatmani, G. Plantard, D. Sacco, I. Aitichou and V. Goetz, Innovative photocatalytic media optimized for solar-powered remediation: application to pyrimethanil, Mater. Sci. Semicond. Process. 16 (2013) 1117-1124. https://doi.org/10.1016/j.mssp.2013.03.004

[65] M. Kacem, V. Goetz, G. Plantard, N. Wery, Modelling aqueous heterogeneous photocatalytic inactivation of Gram-negative Escherichia Coli using suspended and immobilized titanium dioxide reactors, AIChE, 61 (2015) 2532–2542. https://doi.org/10.1002/aic.14834

[66] H.T. Chang, N.M. Wu, F. Zhu, A kinetic model for photocatalytic degradation of organic contaminants in a thin-film TiO_2 catalyst, Water Res. 34 (2000) 407–416. https://doi.org/10.1016/S0043-1354(99)00247-X

[67] T.A. McMurray, J.A. Byrne, P.S.M. Dunlop, J.G.M. Winkelman, B.R. Eggins, E.T. McAdams, Intrinsic kinetics of photocatalytic oxidation of formic and oxalic acid on immobilised TiO_2 films, Appl. Cat. A Gen. 262 (2004) 105–110. https://doi.org/10.1016/j.apcata.2003.11.013

[68] B. Ohtani, S. Adzuma, S. Nishimoto, T. Kagiya, Photocatalytic degradation of polyethylene film by incorporated extra-fine particles of titanium dioxide, Polym. Degrad. Stab. 35 (1992) 53-60. https://doi.org/10.1016/0141-3910(92)90135-R

[69] K. Tennakone, C.T.K. Tilakaratne, I.R.M. Kottegoda, Photocatalytic degradation of organic contaminants in water with TiO_2 supported on polythene films, J. Photochem. Photobiol. A Chem. 87 (1995) 177-179. https://doi.org/10.1016/1010-6030(94)03980-9

[70] K.E.Varner, K. Rindfusz, A. Gaglione, E. Viveiros, Nano titanium dioxide environmental matters: state of the science literature review, U.S. Environmental Protection Agency, Washington, DC, EPA/600/R-10/089, 2010 https://cfpub.epa.gov/si/si_public_record_report.cfm?Lab=NERL&dirEntryId=227225 (accessed September 2010)

[71] U.S. EPA. Nanomaterial case studies: nanoscale titanium dioxide in water treatment and in topical sunscreen (Final). U.S. Environmental Protection Agency, Washington, DC, EPA/600/R-09/057F, 2010 https://cfpub.epa.gov/ncea/risk/recordisplay.cfm?deid=230972 (accessed November 2010)

[72] E.J. Park, H.S. Yoon, D.H. Kim, Y.H. Kim, Y.D. Kim, Preparation of self-cleaning surfaces with a dual functionality of superhydrophobicity and photocatalytic activity, Appl. Surf. Sci. 319 (2014) 367–371. https://doi.org/10.1016/j.apsusc.2014.07.122

[73] R. Sun, A. Nakajima, A. Fujishima, T. Watanabe, K. Hashimoto, Photoinduced surface wettability conversion of ZnO and TiO_2 thin films, J. Phys. Chem. B. 105 (2001) 1984–1990. https://doi.org/10.1021/jp002525j

[74] Q.F. Xu, Y. Liu, F.J. Lin, B. Mondal, A.M. Lyons, Superhydrophobic TiO_2-polymer nanocomposite surface with UV-induced reversible wettability and self-cleaning properties, ACS Appl. Mater. Interfaces 5 (2013) 8915–8924. https://doi.org/10.1021/am401668y

Table 1. Experimental conditions (i.e., NPs concentration in the starting dispersion and deposition time) used for the aerosol-assisted plasma deposition of hydrocarbon polymer/TiO_2 NPs nanocomposite coatings on flat glass slides (22 mm diameter, 0.2 mm thickness, Fig. 1b) and macroporous PU foam samples (22 mm diameter, 4 mm thickness, Fig. 1c). For each set of conditions, the weight of the coating deposited on the selected supporting substrate and the

surface density of the coating are provided. Electrical parameters used for DBD generation were kept fixed for all experiments (i.e., 22 kHz excitation frequency, 2.6 kV_{rms} applied voltage, 50 Hz modulation frequency, 65% duty cycle).

Supporting substrate	[NPs] in the starting dispersion (wt%)	Deposition time (min)	Coating weight (µg)	Coating surface density (µg·mm^{-2})
Glass slide	3	10	300 ± 30	0.79 ± 0.08
	3	30	1000 ± 100	2.6 ± 0.3
	3	60	2100 ± 300	5.5 ± 0.8
PU foam	3	30	650 ± 60	0.077 ± 0.007
	3	60	1300 ± 100	0.155 ± 0.012
	5	30	850 ± 60	0.101 ± 0.007
	5	60	1700 ± 200	0.20 ± 0.02
	8	30	1150 ± 100	0.137 ± 0.012
	8	60	2300 ± 300	0.27 ± 0.04

Table 2. XPS surface atomic concentrations of PU foam samples plasma-coated for 30 and 60 min using dispersions of oleate-capped TiO_2 NPs in a n-octane/1,7-octadiene solvent mixture at concentration of 3, 5 and 8 wt%. The XPS elemental composition of the pristine foam is as follows: C (74 ± 4%), O (20.5 ± 1.0%), N (4.5 ± 0.5%), Si (1.0 ± 0.2%).

Deposition conditions: [NPs], t_d	Analyzed position	C (%)	O (%)	Ti (%)
3 wt%, 30 min	Cross-section	97 ± 2	2.5 ± 0.5	0.5 ± 0.1

	Top	98 ± 2	1.5 ± 0.5	0.5 ± 0.1
3 wt%. 60 min	Cross-section	98 ± 2	1.5 ± 0.5	0.5 ± 0.2
	Top	97 ± 2	2.5 ± 0.5	0.5 ± 0.2
5 wt%, 30 min	Cross-section	94 ± 2	5.0 ± 1.0	1.0 ± 0.3
	Top	94 ± 4	5.0 ± 1.0	1.0 ± 0.5
5 wt%, 60 min	Cross-section	95 ± 4	4.0 ± 1.0	1.0 ± 0.5
	Top	93 ± 3	5.5 ± 1.0	1.5 ± 0.5
8 wt%, 30 min	Cross-section	93 ± 2	5.0 ± 1.0	2.0 ± 0.4
	Top	81 ± 5	14 ± 2	5.0 ± 1.0
8 wt%, 60 min	Cross-section	93 ± 2	5.0 ± 1.0	2.0 ± 0.5
	Top	81 ± 5	14 ± 2	5.0 ± 1.0

Table 3. XPS surface atomic concentrations and WCA values of the best-performing plasma-coated glass slide as prepared and after two and twenty photocatalytic runs, corresponding respectively to 4 h and 40 h of operation under UV light irradiation. The NC coating was deposited on the supporting substrate for 60 min using a DBD fed with He and the aerosol of a 3 wt% oleate-capped TiO_2 NPs dispersion.

Plasma-coated glass slide	C (%)	O (%)	Ti (%)	WCA (°)
As deposited	87 ± 4	10.0 ± 1.0	3.0 ± 0.4	160 ± 3
After 2 reaction runs	56 ± 2	33.0 ± 1.0	11.0 ± 0.5	140 ± 3
After 20 reaction runs	30 ± 3	51 ± 2	19.0 ± 1.0	< 5

Table 4. Curve-fitting results of the high-resolution XPS C 1s spectra of the best-performing plasma-coated glass slide as prepared and after two and twenty photocatalytic runs, corresponding respectively to 4 h and 40 h of operation under UV light irradiation. The NC coating was deposited on the supporting substrate for 60 min using a DBD fed with He and the aerosol of a 3 wt% oleate-capped TiO_2 NPs dispersion.

Plasma-coated glass slide	C-C/C-H (%)	C-O (%)	C=O/O-C-O (%)	COO (%)
As deposited	96 ± 2	4.0 ± 0.4	---	---
After 2 reaction runs	82 ± 4	10.0 ± 0.5	4.0 ± 0.4	4.0 ± 0.4
After 20 reaction runs	81 ± 4	9.0 ± 0.5	2.0 ± 0.3	8.0 ± 0.4

Table 5. XPS surface atomic concentrations and WCA values of the best-performing plasma-coated foam sample as prepared and after two and twenty photocatalytic runs, corresponding respectively to 4 h and 40 h of operation under UV light irradiation. The NC coating was deposited on the supporting substrate for 60 min using a DBD fed with He and the aerosol of an 8 wt% oleate-capped TiO_2 NPs dispersion.

Plasma-coated PU foam sample	Analyzed position	C (%)	O (%)	Ti (%)	N (%)	WCA (°)
As deposited	Cross-section	93 ± 2	5.0 ± 1.0	2.0 ± 0.5	---	
	Top	81± 5	14 ± 2	5.0 ± 1.0	---	155 ± 5
After 2 reaction runs	Cross-section	82 ± 5	14 ± 2	4.0 ± 0.8	---	
	Top	57 ± 3	32 ± 2	10.0 ± 0.5	1.0 ± 0.2	120 ± 10
After 20 reaction runs	Cross-section	73 ± 4	21 ± 3	3.0 ± 0.5	3.0 ± 0.5	
	Top	57 ± 2	32 ± 2	8.0 ± 1.0	3.0 ± 0.3	80 ± 20

Figure captions

Fig. 1. (a) Simplified scheme of the parallel plate DBD system used for the aerosol-assisted deposition of nanocomposite coatings. Representative pictures of the supporting substrates used

in this work before and after thin film deposition: (b) borosilicate glass slide (22 mm diameter, 0.2 mm thickness), (c) open-cell polyurethane foam (22 mm diameter, 4 mm thickness).

Fig. 2. (a) Schematic of the photocatalytic experimental set-up operating in recirculation batch mode and consisting of a photocatalytic cell connected to a peristaltic pump and an optical detector. (b) Photograph of the photocatalytic cell containing a PU foam sample during UV light irradiation.

Fig. 3. (a) ATR-FTIR spectrum, (b) high-resolution XPS C 1s, O 1s and Ti 2p spectra, (c) top-view (left) and cross-sectional (right) SEM images of the NC coating deposited on flat supporting substrates for 60 min in a DBD fed with He and the aerosol of a 3 wt% oleate-capped TiO_2 NPs dispersion in n-octane/1,7-octadiene mixture.

Fig. 4. High-resolution XPS C 1s, O 1s and Ti 2p spectra of the best-performing plasma-coated foam sample (sample interior) before and after use in photocatalytic water treatment under UV light irradiation: (a) as deposited sample, (b) sample after two reaction runs, (c) sample after twenty reaction runs. The NC coating was deposited on the supporting substrate for 60 min using a DBD fed with He and the aerosol of an 8 wt% oleate-capped TiO_2 NPs dispersion.

Fig. 5. Representative SEM images of PU foam samples: (a,c,e) pristine sample, (b,d,f) foam sample coated with a NC thin film deposited by DBD using a 3 wt% oleate-capped TiO_2 NPs dispersion and a deposition time of 60 min. Images of the plasma-coated foam are taken in the sample interior (i.e., cross-section).

Fig. 6. SEM images taken in the interior (i.e., cross-section) of the plasma-coated foam samples prepared using different oleate-capped TiO_2 NPs concentrations in the starting dispersion and

deposition times: (a,b) [NPs] = 3 wt%, t_d = 30 min, (c,d) [NPs] = 8 wt%, t_d = 30 min, (e,f) [NPs] = 8 wt%, t_d = 60 min.

Fig. 7. Residual concentration ratio of methyl orange as a function of the irradiation time using the following samples: (a) pristine glass slide in dark conditions and under UV irradiation (blank experiments), plasma-coated glass slide under UV irradiation ([NPs] in the starting dispersion = 3 wt%, deposition time = 60 min); (b) pristine foam sample in dark conditions and under UV irradiation (blank experiments), plasma-coated foam sample under UV irradiation ([NPs] in the starting dispersion = 8 wt%, deposition time = 60 min). For the plasma-coated samples results from successive photocatalytic runs are reported. (c) Evolution of the MO removal (determined at 75% of the photocatalytic run duration) over successive reaction runs for the plasma-coated glass slide and foam of panels (a) and (b), respectively.

Fig. 8. Apparent kinetic constant (k_{app}) for the methyl orange photocatalytic degradation using the different plasma-coated glass samples prepared in this work and listed in Table 1 (deposition time = 10-60 min, NPs concentration in the starting dispersion = 3-8 wt%). The k_{app} values refer to the third cycle of use.

Fig. 9. Cross-sectional SEM images of the best-performing plasma-coated flat sample ([NPs] in the dispersion = 3 wt%, deposition time = 60 min) before and after use in photocatalytic water treatment under UV light irradiation: (a) as deposited sample, (c) sample after two reaction runs, (e) sample after twenty reaction runs. SEM images taken at a cross-sectioned ligaments in the interior of the best-performing plasma-coated foam ([NPs] in the dispersion = 8 wt%, deposition time = 60 min) before and after use in photocatalytic water treatment under UV light irradiation: (b) as-deposited sample, (d) after two reaction runs, (f) after twenty reaction runs.

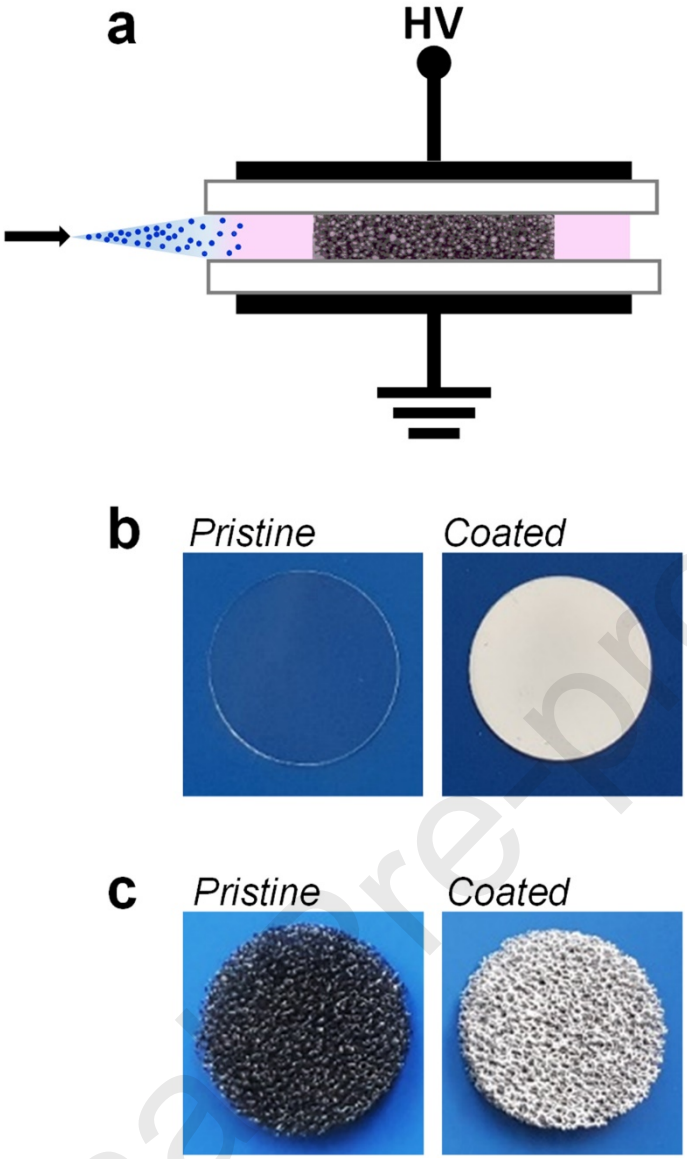

Fig. 1 (color online only)

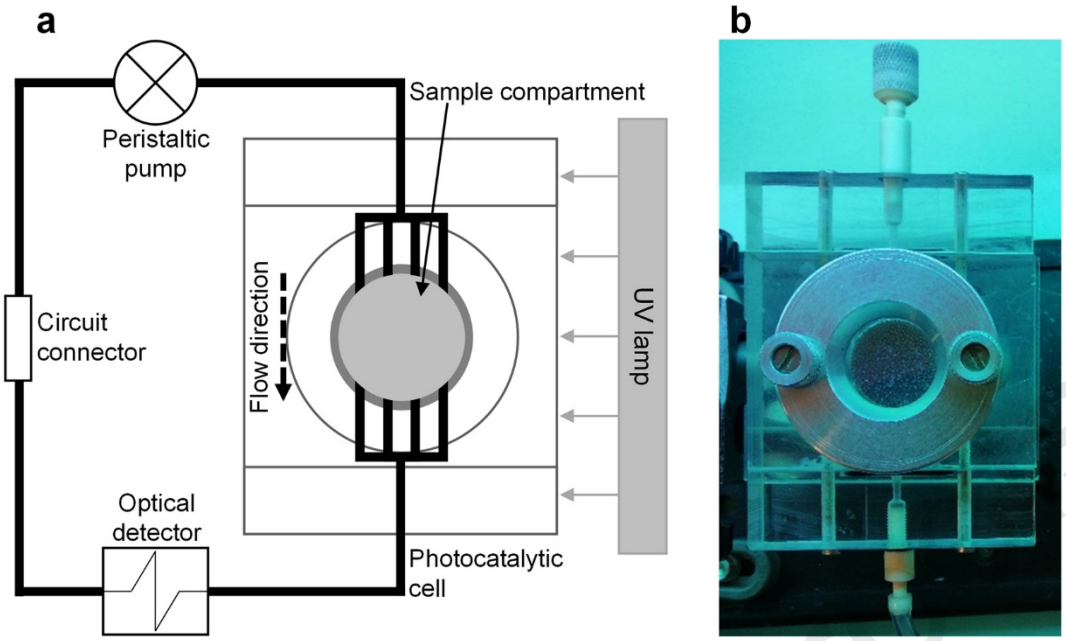

Fig. 2 (color online only)

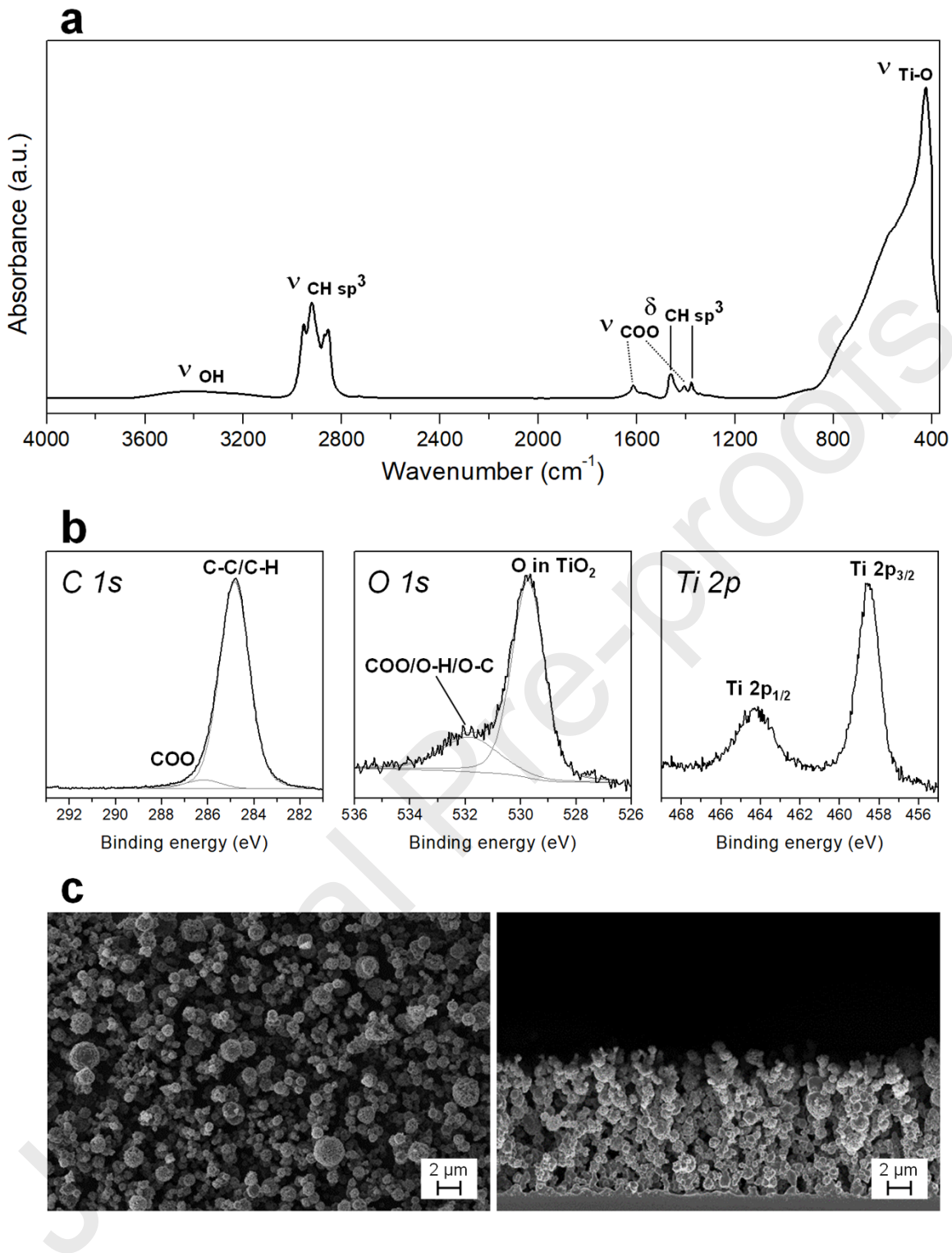
a
Absorbance (a.u.)
ν Ti-O
ν CH sp3
δ CH sp3
ν COO
ν OH
4000
3600
3200
2800
2400
2000
1600
1200
800
400
Wavenumber (cm-1)
b
C 1s
C-C/C-H
COO
292
290
288
286
284
282
Binding energy (eV)
O 1s
O in TiO2
COO/O-H/O-C
536
534
532
530
528
526
Binding energy (eV)
Ti 2p
Ti 2p3/2
Ti 2p1/2
468
466
464
462
460
458
456
Binding energy (eV)
c
2 μm
2 μm

Fig. 3

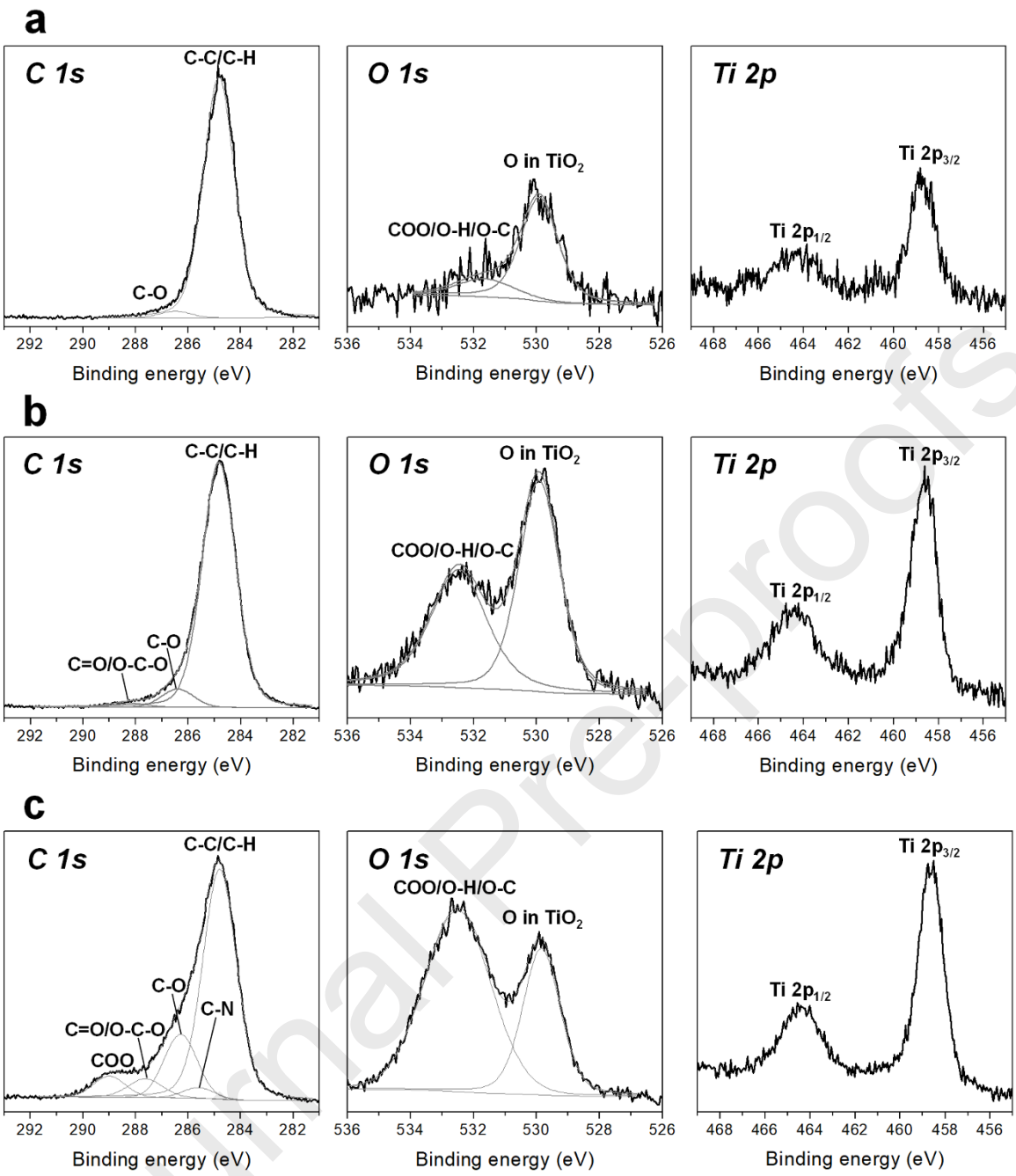
a
C 1s
C-C/C-H
C-O
292 290 288 286 284 282
Binding energy (eV)
O 1s
O in TiO2
COO/O-H/O-C
536 534 532 530 528 526
Binding energy (eV)
Ti 2p
Ti 2p3/2
Ti 2p1/2
468 466 464 462 460 458 456
Binding energy (eV)
b
C 1s
C-C/C-H
C-O
C=O/O-C-O
292 290 288 286 284 282
Binding energy (eV)
O 1s
O in TiO2
COO/O-H/O-C
536 534 532 530 528 526
Binding energy (eV)
Ti 2p
Ti 2p3/2
Ti 2p1/2
468 466 464 462 460 458 456
Binding energy (eV)
c
C 1s
C-C/C-H
C-O
C-N
C=O/O-C-O
COO
292 290 288 286 284 282
Binding energy (eV)
O 1s
COO/O-H/O-C
O in TiO2
536 534 532 530 528 526
Binding energy (eV)
Ti 2p
Ti 2p3/2
Ti 2p1/2
468 466 464 462 460 458 456
Binding energy (eV)

Fig. 4

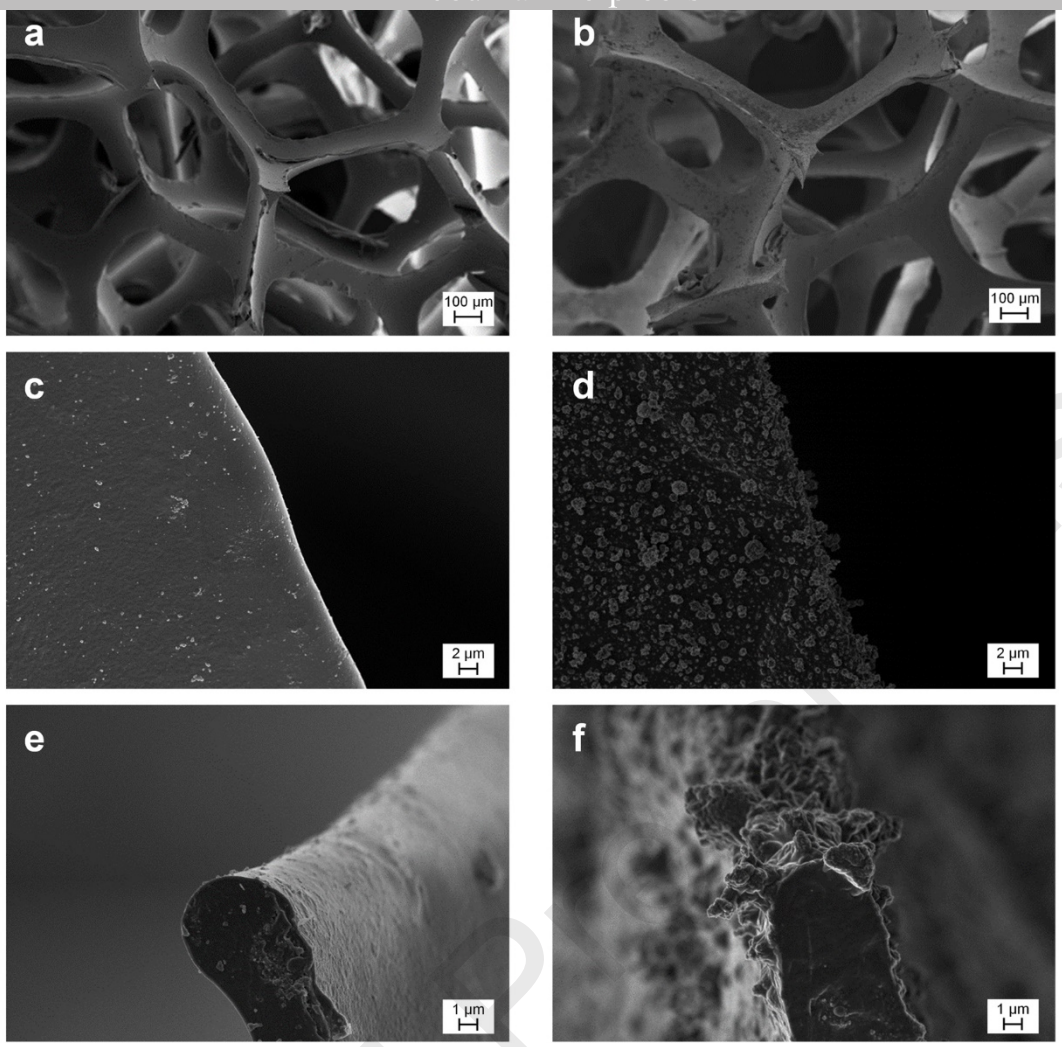

Fig. 5

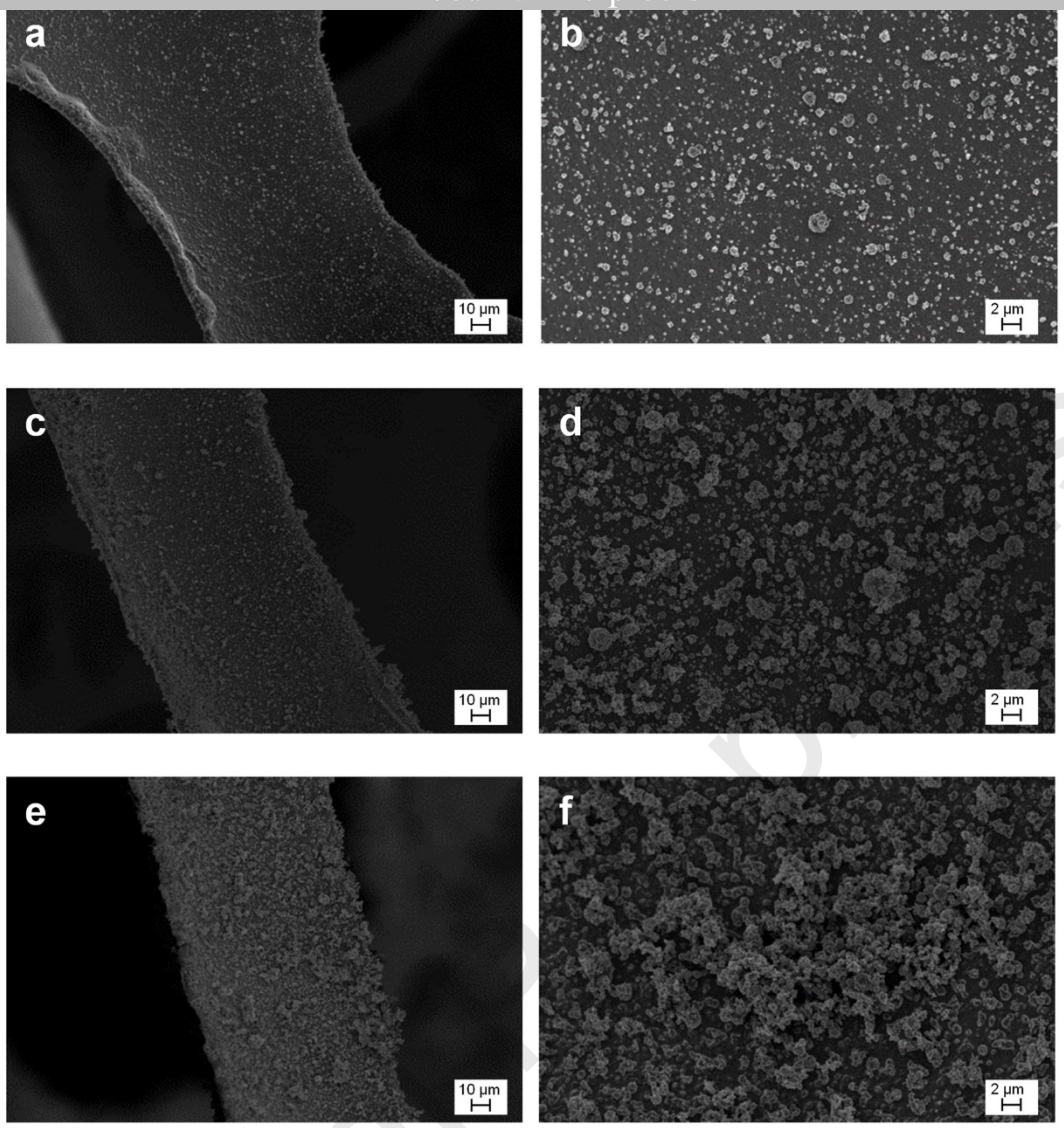

Fig. 6

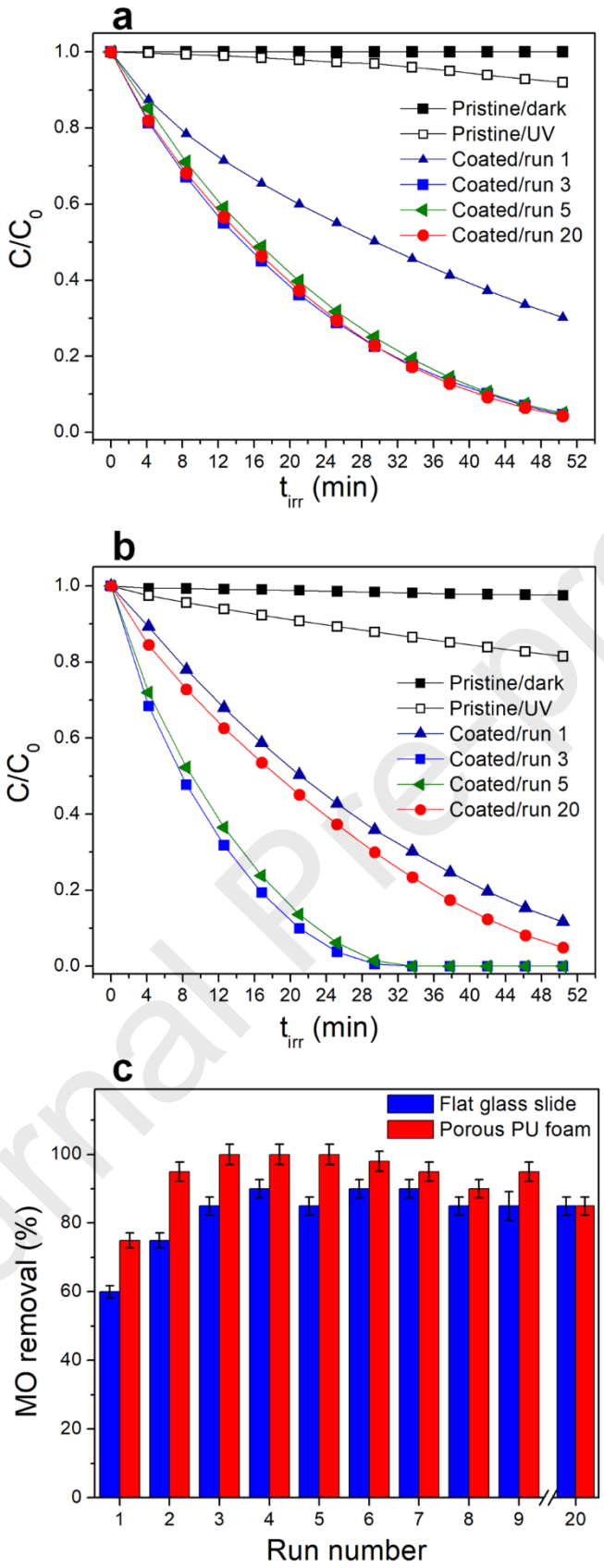

Fig. 7 (color online only)

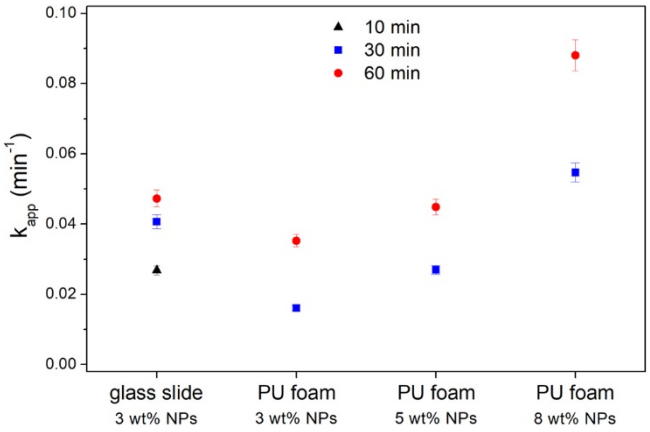

Fig. 8 (color online only)

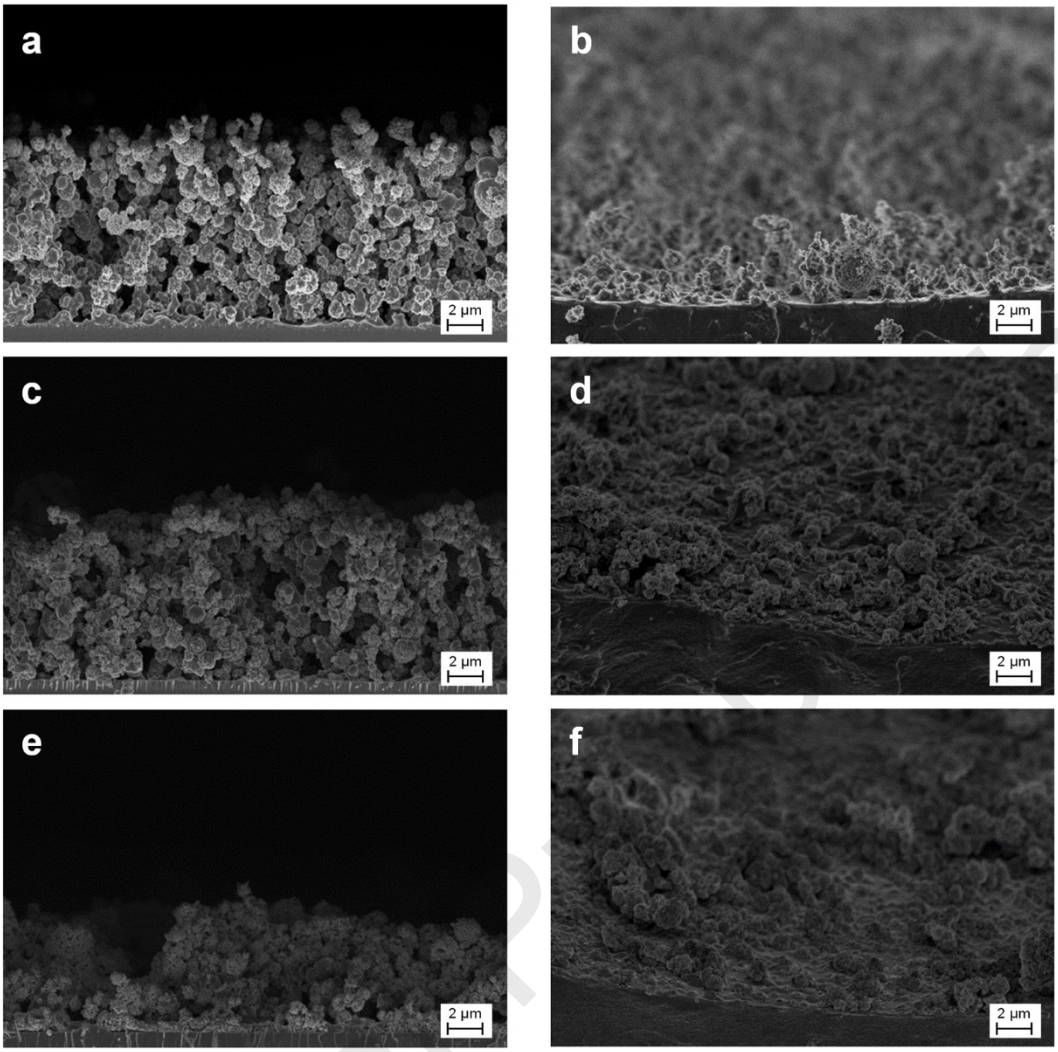

Fig. 9